The SMOS Soil Moisture Retrieval Algorithm

Yann H. Kerr, *Senior Member, IEEE*, Philippe Waldteufel, Philippe Richaume, Jean Pierre Wigneron, *Senior Member, IEEE*, Paolo Ferrazzoli, *Senior Member, IEEE*, Ali Mahmoodi, Ahmad Al Bitar, François Cabot, Claire Gruhier, Silvia Enache Juglea, Delphine Leroux, Arnaud Mialon, and Steven Delwart

***Abstract*—The Soil Moisture and Ocean Salinity (SMOS) mission is European Space Agency (ESA's) second Earth Explorer Opportunity mission, launched in November 2009. It is a joint program between ESA Centre National d'Etudes Spatiales (CNES) and Centro para el Desarrollo Tecnologico Industrial. SMOS carries a single payload, an L-Band 2-D interferometric radiometer in the 1400–1427 MHz protected band. This wavelength penetrates well through the atmosphere, and hence the instrument probes the earth surface emissivity. Surface emissivity can then be related to the moisture content in the first few centimeters of soil, and, after some surface roughness and temperature corrections, to the sea surface salinity over ocean. The goal of the level 2 algorithm is thus to deliver global soil moisture (SM) maps with a desired accuracy of 0.04 m3/m3. To reach this goal, a retrieval algorithm was developed and implemented in the ground segment which processes level 1 to level 2 data. Level 1 consists mainly of angular brightness temperatures (TB), while level 2 consists of geophysical products in swath mode, i.e., as acquired by the sensor during a half orbit from pole to pole. In this context, a group of institutes prepared the SMOS algorithm theoretical basis documents to be used to produce the operational algorithm. The principle of the SM retrieval algorithm is based on an iterative approach which aims at minimizing a cost function. The main component of the cost function is given by the sum of the squared weighted differences between measured and modeled TB data, for a variety of incidence angles. The algorithm finds the best set of the parameters, e.g., SM and vegetation characteristics, which drive the direct TB model and minimizes the cost function. The end user Level 2 SM product contains SM, vegetation opacity, and estimated dielectric constant of any surface, TB computed at 42.5°, flags and quality indices, and other parameters of interest. This paper gives an overview of the algorithm, discusses the caveats, and provides a glimpse of the Cal Val exercises.**

Manuscript received May 27, 2011; revised November 9, 2011; accepted January 8, 2012. Date of publication February 29, 2012; date of current version April 18, 2012. The project was funded by CNES through the TOSCA programme and by RTRA STAE leading to the fruitful collaboration with Eric Wood and the Princeton Team.

Y. H. Kerr is with CESBIO-CNES-CNRS-IRD-Université Toulouse, 31401 Toulouse cedex 9, France (e-mail: Yann.kerr@Cesbio.cnes.fr).

P. Waldteufel is with IPSL/LATMOS, Paris France (e-mail: philippe.waldteufel@aerov.jussieu.fr).

P. Richaume, A. Al Bitar, F. Cabot, C. Gruhier, S. E. Juglea, D. Leroux, and A. Mialon are with CESBIO, 31401 Toulouse, France (e-mail: philippe.richaume@cesbio.cnes.fr; ahmad.albitar@cesbio.cnes.fr; Francois.Cabot@cesbio.cnes.fr; claire.gruhier@cesbio.cnes.fr; silvia.enache@cnes.fr; lerouxd@cesbio.cnes.fr; arnaud.mialon@cesbio.cnes.fr).

J. P. Wigneron is with INRA EPHYSE, 33140 Villenave d'Ornon, France (e-mail: jpwigner@bordeaux.inra.fr).

P. Ferrazzoli is with Tor Vergata University, 00133 Rome Italy (e-mail: ferrazzoli@disp.uniroma2.it).

A. Mahmoodi is with Array Systems Computing Inc., Toronto, ON M3J 3H7, Canada (e-mail: ali@array.ca).

S. Delwart is with ESA ESRIN, 00044 Frascati, Italy (e-mail: steven.delwart@esa.int).

Color versions of one or more of the figures in this paper are available online at http://ieeexplore.ieee.org.

Digital Object Identifier 10.1109/TGRS.2012.2184548

***Index Terms*—Cal/Val, model, SMOS, soil moisture, retrievals, vegetation opacity.**

I. Introduction

L-BAND radiometry has proven to be the most promising remote sensing techniques to monitor soil moisture (SM) over land surfaces and at the global scale [1]–[4]. An improvement in the estimation of the time variations in SM can provide significant improvements in meteorological and hydrological forecasts. In addition, L-Band is used for the estimation of salinity over global ocean surfaces. For these reasons, a number of space missions based on L-band microwave radiometers on satellite platforms have been developed and submitted to national space agencies. The first was Soil Moisture and Ocean Salinity (SMOS), launched in November 2009, was followed by Aquarius in June 2011 and the Soil Moisture Active and Passive (SMAP) is scheduled for 2014. A major goal of these missions is to enable, for the first time, direct and robust quantitative estimates of surface SM over most of the land masses and/or sea surface salinity over oceans. SMOS has two sets of level 2 products, one for ocean surfaces the other one for land. This paper gives an overview of the land surface retrieval algorithm, details of which are provided in the algorithm theoretical basis document (ATBD) [5].

The microwave signal at L-Band is mainly driven by SM, vegetation effects, and the effective surface temperature. The atmosphere and additional surface characteristics, such as soil surface roughness, topography, soil texture, and soil bulk density, have a smaller (second-order) influence. The SM retrieval algorithms, however, need to account for all these various effects.

A distinguishing feature of SMOS is its multi angular measurement capability. This feature allows for the retrieval of additional parameters beyond SM. A classical conical scan radiometer, such as Advanced Microwave Scanning Radiometer (AMSR), scanning multichannel microwave radiometer (SMMR), soil moisture active passive (SMAP), will provide at best one fully polarized measurements for any given point. This makes the retrieval of several surface variables at the same time impossible (more unknowns than equations) unless other measurements are included, leading to the use of other data sources to infer extra required pieces of information (i.e., vegetation opacity or surface temperature for instance). An accurate estimation of the vegetation water content is a key requirement. For this purpose, it is common to establish a relationship between an index such as the normalized difference vegetation index (NDVI) to infer Leaf Area Index (LAI) which in turn is related

to vegetation water content and opacity. This latter relationship is obtained by the use of a vegetation type dependent constant accounting for the vegetation structural characteristics. SMOS has a definite advantage over conical scan radiometers, as it measures the angular signature of the surface and provides up to 160 angular fully polarized measurements, allowing the user to infer both moisture and, directly, vegetation opacity. Before settling on iterative approach using forward models, several approaches including neural networks and statistical or semi-empirical/empirical methods were considered. They were not selected as it seemed premature to derive statistical methods when no previous experience of such L-Band retrievals of SM at a spatial resolution of 40 km was available. Consequently, establishing a global relationship between surface "known" values and satellite brightness temperatures (TB) seemed a very challenging goal, and the option taken was to rely on state of the art physically based algorithms as the retrieval algorithm had to be operational soon after SMOS launch.

Based on L-Band measurements from airborne or ground-based observation systems, several studies have investigated the effects of the vegetation canopy [6]–[11], as well as the effects of soil temperature [12], [13], snow cover [14]–[17], topography, and soil surface roughness [18], [20], [21]. Several retrieval algorithms have also been proposed in the literature [2], [9], [11], [21]–[25]. Since the 70's with the SMMR, many authors have developed and tested various algorithms, the most successful attempts being made with low-frequency systems (C-band around 5 cm wavelength and, 5 GHz). These sensors provided many interesting results but were always hampered by the relative high frequency and therefore not sensitive enough when the vegetation became dense [26]. L-Band seemed the best way to go, and as soon as tractable solutions became possible for the antenna, the SMOS [27], [28], Aquarius [29], and SMAP [30], [31] concepts emerged. However, as almost no space-borne L-Band observations were available yet (with the notable exception of Skylab which was flown in 1974 and provided a limited sample of data at a rather coarse spatial resolution), the SM retrieval approaches could not be tested with real data. Results gained from higher frequency missions, and ground-airborne based experiments were "scaled" to L-Band using ad hoc methods. The SMOS retrieval algorithm had thus to be developed based on ground experiments and modeling activities only, and it was only after the SMOS launch, with real data, that the actual efficiency could be ascertained. Currently, through calibration and validation exercises, the algorithm based on the use of the target's angular signature, is undergoing improvements so as to cover more of the land mass.

To summarize the retrieval algorithm first identifies the earth surface area (or the target) responsible for shaping a particular set of SMOS signals, i.e., the set of TBs corresponding to multi-angular views of a single target [32]. This target is considered as a collection of units, or surface elements, each specified by its surface characteristics (or state) and its position within the target area. Since SMOS sees the target from different angles the contribution of a given surface unit to the signal usually varies from one view to the next. The amount of contribution for a given unit is controlled by its state at a given time (captured by a forward model), its position, and the antenna pattern (both of which are captured by a weighting function for the given incidence angle). The collective contributions from all units and other sources, like sky and atmosphere, is what shapes the signal for a given angle. The retrieval algorithm, while it assumes "known" states for certain units (known as default contribution) attempts to "guess" the states of others in order to arrive at what is observed by SMOS. In this attempt, the algorithm, in an orderly fashion, adjusts the parameters that control the states of each unit in order to minimize the "distance" between the observed and modeled signal derived from the last best guess. The parameters that define the state of each elementary unit include SM and vegetation optical thickness. This paper describes in details various elements of the above algorithm.

II. Overview of the Input Data

The retrieval algorithm is designed to use, as input, SMOS Level 1c (L1c) product. SMOS characteristics are given in [32]–[34] and are summarized in this section. The basic resolution (3-dB half power beam width) corresponds to a 43-km foot print on average (maximum 27 km minimum 55 km over the field of view for continental areas) The footprint shape varies with angle [33] making the common term of pixel ambiguous. As we are dealing with multi-angular measurements, each having a different footprint, it is often better to refer them by their center called the node. The L1c product is provided over the ISEA-4H9 (icosahedral snyder equal area Earth fixed) grid referred to as the discrete global grid (DGG). The nodes are equally spaced at 14.989 km. Products for descending and ascending half-orbits are separated. They include all possible land nodes with a margin over sea bodies. The geolocation accuracy of SMOS is typically 500 m. Geolocation bias due to launch shift and arms deployment was calibrated within the first 6 months in orbit, fitting a linear coastline to the observed transition in SMOS data. Given the spatial resolution of the instrument and the selected method, the accuracy of this calibration has been assessed to be slightly better than 500 m [36].

The level 2 (L2) inversion is done over each DGG node independently and is delivered on the same ISEA-4H9 grid for the European Space Agency (ESA) products. Although SMOS pixels, given in the L1c product for a DGG node, are associated with a single earth-fixed area centered on that DGG node, it is not always the same area on the ground which is seen from various angles. This is due to the earth sphericity and the fact that conical solid angle intercepts the earth over a distorted ellipse whose main axis changes with azimuth and view angle. This phenomenon is not new and has been encountered with other systems, the extreme case being obtained for the scatterometer. The revisit time is 3 days at the equator for both ascending and descending passes which are sun synchronous at 6 am ascending (resp. 6pm descending). Since the end of the commissioning phase, data are acquired in full polarization mode, i.e., the four Stokes' components are obtained including Stokes' 3 and 4. The ground sampling is of $\approx$15 km. Every 2.4 s, a full set of polarizations is acquired.

The L2 SM retrieval algorithm uses two types of auxiliary data files: so called **static** and **dynamic**. The static data do not vary over time or have slowly varying quantities. They include the soil texture maps from FAO [37], the land use maps from ECOCLIMAP [38], and the topography index [20].

The dynamic data provide time varying quantities (snow, freeze defreeze, rain, temperature) and are obtained from the European Centre for Medium Range Weather Forecasts (ECMWF) forecasts.

Finally, some quantities are not readily available but can be inferred from the inversion process. Those are in the so-called "current" files which include vegetation opacity, surface roughness, and radio frequency interferences (RFI) indicators. The "current" files are updated regularly based on SMOS observations and are used as inputs for future inversions. The vegetation optical thickness is a time varying quantity, initially estimated based on the LAI provided in ECOCLIMAP and then through "current" files.

III. Soil Moisture Retrieval Approach

A. Rationale

The signal measured by a passive microwave sensor at L-Band, over a nonfrozen and snow free surface, is mainly a function of SM, vegetation opacity, and effective surface temperature. Other surface characteristics like soil texture and roughness also play an important role. Atmospheric contribution (including clouds and rain), galactic reflection, can be easily neglected over land surfaces.

At the SMOS resolution (40 km on average), the surface responsible for shaping the L-Band signal is rarely uniform. A surface area responsible for shaping the SMOS pixel often consists of some water bodies, low and possibly high vegetation fields, possibly frozen and snow-covered surfaces, topography, and others. Consequently, any physically based retrieval algorithm has to be able to account for a number of features in the observed area. Some surface characteristics, like soil texture and land use, are obtained from static maps while others, like temperature and snow, are obtained from forecasts. A significant challenge is therefore to determine with an adequate accuracy and globally the surface characteristics and use them in the retrieval process to infer the desired ones.

In order to capture the effects of a wide range of parameters, it was decided to endeavor to use models as exhaustive and comprehensive as possible with the assumption that it would always be possible to simplify at a later stage should any model component prove to bring very a negligible improvement during the validation process. For instance, the single scattering albedo formulation is exhaustive but very seldom used in all its complexity [5].

Consequently, the retrieval algorithm is physically based using state-of-the-art models and was designed to be robust and easily improved. During the first month of operations, some features proved to be unnecessary while others required attention. The overall results, however, were very satisfactory from the beginning. We can also state that there is still substantial room for improvements. The most disappointing discovery was the existence of unexpectedly strong RFI level in some areas of the world where intensive cal Val sites had been painstakingly implemented.

B. Core of the Challenge: Dealing With Inhomogeneous Areas

The SMOS Level 2 algorithm is based on an iterative approach which aims at minimizing a cost function whose main component is the sum of the squared weighted differences between measured and modeled TB data, for a collection of incidence angles. This is achieved by finding the best-suited set of the parameters, which drive the direct TB model, e.g., SM, and vegetation characteristics.

Despite the apparent simplicity of the SM retrieval principle, the modeling of the radiometric signal is complex and requires close attention to many details. The SMOS "pixels" can correspond to rather large, inhomogeneous surface involving many parts each with its own characteristics. Moreover, the radiometric signal is impacted by the directional pattern of the SMOS interferometric radiometer. Therefore, modeling of the SMOS radiometric signal involves both the modeling of the ground target and the antenna for a variety of incidence angles. The modeling of the ground target involves estimation of various parameters (like surface temperature and SM) at various positions within the target. The antenna pattern is represented through a weighting function which depends on the incidence angle. It is important to note that, thanks to the "reconstruction" principle, any given point of the surface is always seen with exactly (to the pointing knowledge accuracy of 400 m) the same center. Hence, from one acquisition to any other, surfaces seen are always the same.

The primary objective of the SMOS Level 2 SM algorithm is to retrieve SM over fairly large (40 km typically) and thus inhomogeneous areas. Obviously, over any pixel, there is a large variety of surface types, not all of which are characterized by the same set of parameters and therefore not realistic to carry out the same retrieval everywhere. It is understood that all surface types, regardless of whether they support the retrieval of a given set of parameters, do contribute to the SMOS signal according to a given model. However, estimation of SM is only meaningful over certain surface types. For instance, while a lake contributes to the radiometric signal, it is not parameterized by SM. In order to facilitate the retrieval process, a node is divided generally in two areas, one where the retrieval will take place and one where the contributions to the overall node signal need to be estimated but no retrievals will be performed. This latter part is then considered to have fixed (**default contributions**), and the retrieval is made on the remaining—**dominant**—area. For instance, if there is an area of low vegetation with a dense forest and a lake, we will estimate the contribution of the lake and that of the forest using either external data or predetermined values of the surface characteristics: the **reference values**. This default contribution will be assumed constant in the modeled signal, and the retrieval is performed only on the remaining, dominant part.

In order to determine the dominant part, an average weighing function (mean foot print) coupled with a high-resolution land

use are used. The output of this process indicates what fractions are available in the target area and which parameters are required to characterize each fraction. This information is then used as input to a decision tree which, step by step, selects the type of model to be used according to surface conditions. Hence, the basic principle is to divide the target area into a finite and small number of categories. The main categories are surfaces with low vegetation ("low" meaning height not exceeding 1 to 2 m as compared to trees), forested areas, barren land (rocks), water bodies, urban areas, permanent ice, and snow. Also, included are varying surfaces (i.e., seasonally covered with snow). Each target area is decomposed into 4-km cells for which the land use is assessed from the ECOCLIMAP database. Using the mean foot print, it is possible to assess the dominant land use as well as the main secondary land uses. For instance, a node might be 78% low vegetation, 14% forested, 7% water, 1% urban. Using the decision tree, the algorithm will do the retrieval (as explained below) only for the low vegetation part. For other fractions, their "default" contributions is computed.

A surface area contributing to SMOS signal usually includes large variety of surface types, like cultivated agriculture, grasslands, and forests. These land use classes are grouped together based on their L-Band microwave emission properties. All surface types are aggregated into a small number (about 10) of generic classes having the same modeling characteristics and using similar parameters. A target area, identified by a DGG node, is subdivided into a number of units (4 km^2 by default), and each unit is defined by a collection of such aggregated fractions. The SMOS pixels geolocated to the node, identifying this target area, correspond to various views of this target as seen from different angles. The spatial extents of two different views from the same target are normally different. The difference normally increases as the viewing angles are further apart. For instance, a forest on the border might appear in some views and not in others (i.e., the extent of "forest" fraction in a target depends on incidence).

The dominant part does not always cover nice rolling hills of green pastures (also known as "nominal"). The soil can be frozen or covered with snow or rocks. The target could be an island within a sea or have a large urban or mountainous component, not to forget marshes or rice fields. These non-nominal, or exotic, cases need to be modeled differently. The exotic surfaces could be either complementary (i.e., there is no overlap between two classes of this type) or supplementary (it necessarily overlaps with complementary classes). For instance, surface characteristics can be supplementary when two "special" cases are present at the same place and same moment (i.e., topography and water body or forest). They can be supplementary when they exclude one another such as water body and forest.

When it is not possible or relevant to retrieve SM, it may be possible to retrieve other parameters of interest. For instance one can retrieve dielectric constant parameter (using the so-called Cardioid approach).

In addition, the algorithms compute modeled TB at a fixed angle once the retrieval has converged. It uses the set of parameters obtained at the end of the retrieval process as input to forward models to compute TB values for both polarizations are the surface and at the antenna frame. The fixed angle is currently set to 42.5°.

C. Implementation

The SM retrieval is based on a Bayesian approach to retrieve SM. For each grid node, a working area (WA) of 123 × 123 km is considered. This is assumed to be the maximum area extent contributing to the SMOS signal for the given node. This area is centered on a given DGG node and is subdivided into approximately 35 × 35 cells (also known as discrete fine flexible grid or DFFG for short) of approximately 4 km^2 each. The TB seen by SMOS is assumed to be the collective contributions from elementary DFFG cells as weighted by the antenna pattern.

The upwelling set of TB values, one per incidence angle, for each DFFG cell is computed using an L-Band microwave emission of the biosphere (L-MEB) [11]. Each DFFG cell contains a collection of aggregated fractions, and each fraction has an associated (L-MEB) forward model. The L-Band microwave emission from a given fraction is determined by the values of the parameters used in the associated forward model. Such parameters characterize the fraction, and the set of values define the state of the fraction. For instance, the state of the "nominal" soil fraction is defined by its SM, soil temperature, soil roughness, and others. Therefore, each fraction is characterized by a set of parameters whose values define the state of that fraction. The set of parameters can be viewed as a vector.

Each target consists of a large number (35 × 35) of DFFG cells, each of which has at most ten fractions. The sheer number of these makes tasks of determining the state for each aggregated fraction computationally challenging. While the states of fractions with default contribution remain fixed, the states of fractions over which we intend to obtain new information are updated at every iteration until their modeled emissions closely matches that of SMOS. The change of state could only involve a few parameters, like SM or vegetation opacity, but this of course changes the L-Band emission of the surface. As an example if the target within SMOS view contains large agricultural fields together with a small water body, then the state of the water body usually remains fixed while the state of the agricultural fields are adjusted by updating their averaged SM.

In order to determine the incidence angle dependent TB value, the surface emission is convoluted with the antenna weighting functions obtained from the SMOS equivalent antenna pattern. Such TB values are still in the earth surface frame. In order to transfer the polarized TB values to the antenna frame one has to apply rotations due to Faraday (TEC contents) and geometry.

A cost function is defined which measures the "distance" of TB values observed by SMOS at the antenna level and those modeled using L-MEB. The "distance" is essentially the sum, for available incidence angles, of quadratic differences between the observed and modeled TBs, normalized by measurement uncertainties. The cost function also includes terms which depend on prior values and uncertainties on parameters to be retrieved, thus implementing a Bayesian approach. An iterative optimization procedure is then used to minimize the cost function. Successive retrieval attempts with a decreasing

number of parameters to be retrieved are carried out whenever needed.

The SMOS observed TBs for each DGG node are provided in the L1C products. The resolution associated with the TBs varies with the observation angle as the ellipsoidal footprint changes in size and shape. The change in the footprint is taken into consideration in the algorithm via the convolution with the antenna pattern mentioned earlier.

The L2 SM algorithm uses a mean weighting function to characterize the WA associated to a target. The WA is the 123 × 123 km area centered on the DGG node being considered. This allows the algorithm to determine the fractions for which we need to assign a forward model. This mean weighting functions can be considered as the average footprint over all observation angles of SMOS for one DGG node.

The level 2 SM processor provides also a complementary product: the SM level 2 data analysis product. This product contains the description of the surface, the residual TBs between model and measurements (TBLMEB-TBSMOS) and the processors performances (number of iterations, χ^2 coefficient, etc. . .), provided over the same ISEA-4H9 grid.

The vegetation optical thickness is related to the vegetation water content and thus indirectly to LAI. These quantities vary slowly over a period of 3 days over an area of 800 km^2 if no special event (rainfall, tsunamis, flooding. . .) occurs. To enhance the SM retrieval, an initialization of the optical thickness value and its associated uncertainty is done in the processing by using the last (i.e., retrieved during the previous SMOS overpass) or CURRENT value. Using this CURRENT mode enables a lower uncertainty of the optical thickness. In this case, the modeled multi-angular TB signature will be highly dependent on SM retrievals. The current file configuration is also applied to other files for RFIs detection.

IV. Direct Model

Fig. 1 gives an overview (flow chart) of the algorithm. Once the node is characterized the minimization approach requires a radiative transfer model. It was decided to use the state-of-the-art LMEB model [11] with some modifications, improvements, or adaptations. (Figs. 2 and 3)

A. Radiative Transfer Equation

The signal measured at the antenna consists of 4 main components. Combining these four components gives the general **radiative transfer equation** (RTE) [26]:

$$\mathrm{TB_p} = \mathrm{TB_{atu}} + \mathrm{TB_{sp}}\exp(-\tau_{\mathrm{atu}}) + (\mathrm{TB_{atd}} + \mathrm{TB_{sk}}\exp(-\tau_{\mathrm{atd}}))\, r_{\mathrm{sp}}\exp(-\tau_{\mathrm{atu}}). \quad (1)$$

All the terms of the above equation are functions of frequency and incidence angle θ between the line of sight and the local normal to earth surface; the "p" subscript indicates the **polarization**. The "s" subscript refers here to combined (surface + near surface) layers.

The upward and downward path atmospheric opacities τ_{atu} and τ_{atd} depend on the gaseous and liquid droplet attenuating

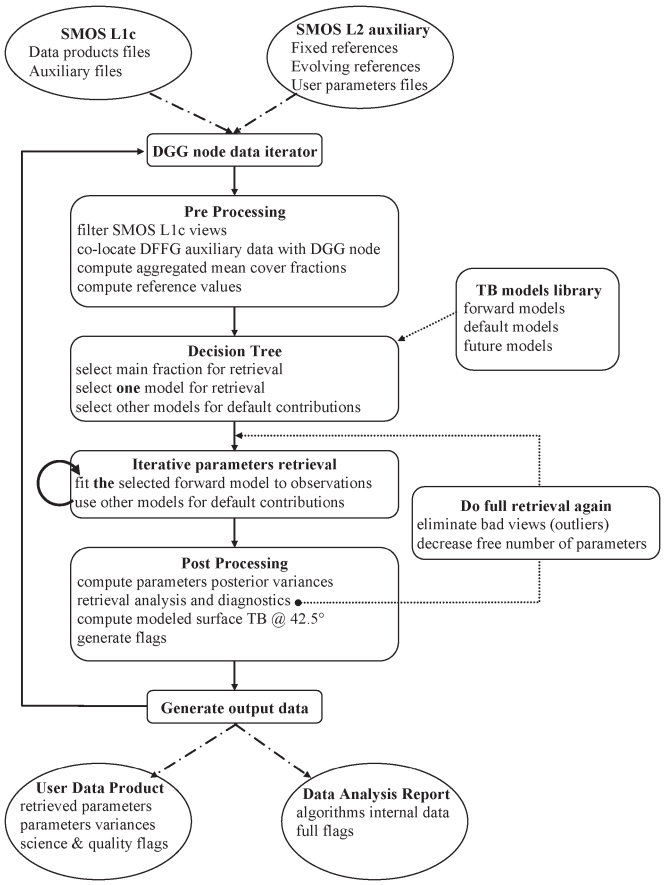

Fig. 1. Flow chart of the level 2 soil moisture retrieval algorithm (from [5]).

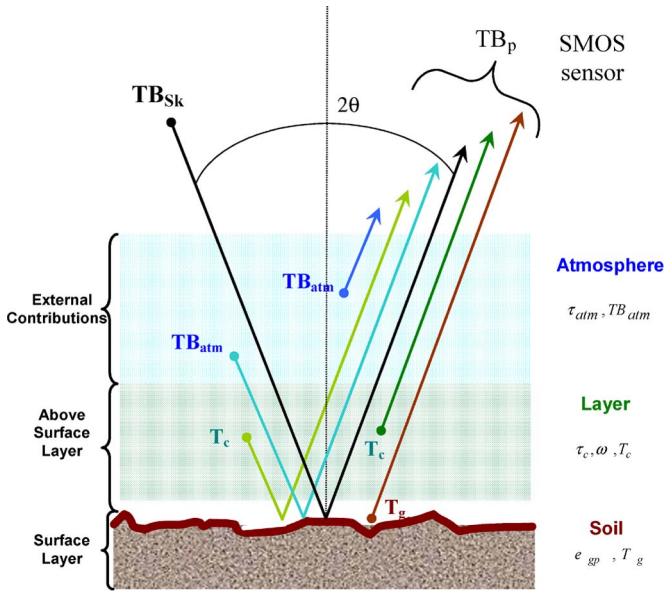

Fig. 2. Contributions to TOA brightness temperature.

constituents (primarily oxygen, water vapor, and clouds) [26]. Considering that we are operating at L-Band, we can safely assume that τ_{atu} and τ_{atd} are almost equal, as differences are linked to differences in atmospheric temperatures and constituents profiles between the two paths. They will be both assigned as τ_{atm}.

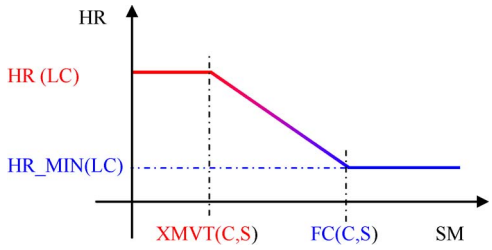

Fig. 3. HR(SM): roughness as a function of SM.

The **surface reflectivity** $r_{\rm sp}$ is assumed to be dominated by the specular component. This approximation is acceptable at L-Band and for not too rough surfaces if nonspecular components are neglected. This variable is the key to what we need to retrieve. Its main influence over the overall brightness lies in its indirect influence on the surface $\mathrm{TB_{sp}}$, since $r_{\rm p}$ is the complement to 1 of emissivity [(2)]. The atmospheric radiation components $\mathrm{TB_{atd}}$ and $\mathrm{TB_{atu}}$ are dependent upon the vertical profiles of temperature, gaseous constituents, and liquid droplets in the atmosphere. Their computation takes into account absorption and scattering. At L-Band, atmospheric effects are small and $\mathrm{TB_{atd}}$ and $\mathrm{TB_{atu}}$ can be considered as equal to $\mathrm{TB_{atm}}$.

At L-Band, the so-called **Faraday rotation**, linked to the columnar electron content (TEC) of the ionosphere over the path, causes the polarization plane to be rotated by, on average, up to a few degrees. This factor has to be taken into account when the TEC (hence the effect) is high (afternoon pass, high solar activity/bursts).

Finally, $\mathrm{TB_{sk}}$ is the **sky background**. At L-Band, several sources are present; the galactic plane contains a number of significant sources that might have to be accounted for. One should not forget the **Sun**, which at L-Band is a very significant source (100 000 to 300 000 K) and will have to be considered.

Surface variables such as temperature, roughness, vegetation, snow, etc... enter the general RTE through their effects on surface reflectivity $r_{\rm sp}$ and surface TB $\mathrm{TB_{sp}}$:

$$\mathrm{TB_{sp}} = e_{\rm sp}\, T_{\rm s} \tag{2}$$

where $e_{\rm sp}$ is the **surface emissivity** $(e_{sp} \cong 1 - r_{sp})$ and $T_{\rm s}$ is the **effective** (physical) surface temperature.

For **bare soil** surfaces, $T_{\rm s}$ reduces to a weighted sum $T_{\rm g}$ of soil temperatures at subsurface levels accounting for the penetration depth.

B. Aggregated Radiative Transfer Equation

At the SMOS scale (25–60 km), pixels are not uniform, and we may have a variety of surface types, for instance, a rural area with towns and roads, bare fields, fallow land and some crops, thickets or woodland, the occasional river or pond, and again, in the worst case, snow here and there with frozen grounds in some places.

In such cases, the total TB comes from several classes of emitters. This composite TB is obtained through an **aggregated** forward model that combines each class of emitting sources weighted by their intrapixel cover **fractions**.

To show clearly how this aggregation is done, for given polarization and incidence angle and a **homogeneous** L1c scene, we first rewrite (1) assuming that downwards and upward atmospheric contributions are equal:

$$\begin{aligned}\mathrm{TB_p} = {} & \mathrm{TB_{atm}} + \exp(-\tau_{\rm atm})\,[\mathrm{TB_{atm}} \\ & + \mathrm{TB_{sk}}\exp(-\tau_{\rm atm})]\, r_{\rm gp}\exp(-2\tau_{\rm c}) \\ & + \exp(-\tau_{\rm atm})\,[e_{\rm gp}T_{\rm g}\exp(-\tau_{\rm c}) \\ & + T_{\rm c}(1-\omega)\,(1-\exp(-\tau_{\rm c}))\,(1+r_{\rm gp}\exp(-\tau_{\rm c}))]\,. \end{aligned} \tag{3}$$

The reflectivities and emissivities $r_{\rm gp}$ and $e_{\rm gp}$ include both smooth surface effects from the dielectric constant and roughness effects. The method to build a single physical temperature parameter from $T_{\rm g}$ and $T_{\rm c}$ is discussed below.

In the description of atmospheric contribution, we refer to an equivalent physical layer temperature, linked very simply to $\mathrm{TB_{atm}}$ and $\tau_{\rm atm}$.

Many terms and factors in this expression depend on polarization and incidence angle. This is detailed in forward models below.

Consider now a **mixed** L1c scene with $n = 1$ to NF **mean** (over incidence angle) fractions $\mathrm{FM_n}$. Of course, NF is actually a small number. For each L1c view, **incidence angle-dependent** values $\mathrm{FV_n}$ for fractions are to be computed.

For ease of writing, we rewrite (3) as follows:

$$\begin{aligned}\mathrm{TB_p} = {} & \mathrm{TB_{atm}} + \exp(-\tau_{\rm atm})\,[\mathrm{TB_{atm}} \\ & + \mathrm{TB_{sk}}\exp(-\tau_{\rm atm})]\,\mathrm{R1} + \exp(-\tau_{\rm atm})\mathrm{R2} \end{aligned} \tag{4}$$

where only the expressions $R1 = r_{\rm gp}\exp(-2\tau_{\rm c})$ (dimensionless) and $R2 = e_{\rm gp}T_{\rm g}\exp(-\tau_{\rm c}) + T_{\rm c}(1-\omega)(1-\exp(-\tau_{\rm c}))(1+r_{\rm gp}\exp(-\tau_{\rm c}))$ (in Kelvin) depend on the fraction n. Then, the **aggregated** forward model, for each view, is derived from (3) where:

$$\mathrm{R1\ becomes:}$$

$$\mathrm{R1} = \sum_{n=1}^{\mathrm{NF}} (\mathrm{FV_n\ R1_n})$$

$$\mathrm{R2} = \sum_{\mathrm{n=1}}^{\mathrm{NF}} (\mathrm{FV_n\ R2_n}).$$

C. Towards Elementary Radiative Models

In the following, elementary radiative models are described whenever available. If no model exists (i.e., urban), it was decided to put a placeholder with a proxy model (in this case some sort of a bare soil). Then:

- The first goal is to retrieve SM over areas devoid of strong topographic features, possibly covered by low vegetation, for which volume surface moisture can be defined. This will be called the **nominal** SMOS target (in short NO for nominal, or LV for low vegetation). Forward models are available.

- It may happen that, although SM is in principle relevant, forward models are poorly known or not validated. This is e.g., the case for strong topography, snow cover.
- In some cases, SM is no longer relevant. Examples are open water, ice.

We will now summarize the details of nominal models as well as other cases.

The nominal case develops the way to model surface roughness as well as the vegetation layer. Note that

- surface roughness is also present for other cases excepting all water surfaces;
- vegetation layer is also present for other cases, excepting free water surfaces but including wetlands

1) For the Nominal Case (Vegetated Soil): The modeling approach used here relies on an extensive review of current knowledge and previous studies. It accounts for, as much as possible, emission from various land covers, from bare soil to full vegetation-covered surfaces, snow-covered surfaces, open water, and atmospheric effects.

The **nominal case** consists of "normal" soil with low vegetation, eventually a manageable amount of free water. The "manageability" is expressed by **thresholds** for which values are suggested in the decision tree section but will often require confirmation.

We will consider several classes in the general approach with two main parts: low vegetation (grassland, crops, etc.) and forest vegetation (coniferous, and broadleaf).

a) Bare soil: Bare soils are quasi-opaque at 1.4 GHz, so the radiative budget is mainly ruled by their emissivity e and reflectivity r, for each polarization p, with:

$$e_{gp} + r_{gp} = 1. \tag{5}$$

The emission of microwave energy is governed by the product of the soil effective temperature, $T_{\rm s}$, and soil emissivity, $e_{\rm gp}$. At L-Band, the emissivity $e_{\rm gp}$ is in turn is a function of the soil's characteristics, i.e., moisture, texture, roughness, and eventually salinity.

Bare soil is simulated using Fresnel laws with either Dobson's formulation for dielectric constants [39], [40] or Mironov's formulation [41]–[43]. The latter was implemented as Dobson's model is not fully adequate at low frequencies (1.4 GHz) particularly in the case hot sandy soils.

The quantities required for the model inputs are derived from the soil's map. As soils are typically rough, we used a modified Wang Choudhury's [44], [45] formulation for roughness with a modification notably in relation to the exponent 2 replaced by NRp as suggested by Escorihuela *et al.* [46]. Consequently, as surface roughness increases, the angular signature of TB is affected, requiring correcting the Fresnel law with the following empirical phenomenological expression:

$$r_{gp}(\theta) = ((1 - \mathrm{QR})r_{bp} + \mathrm{QR}\, r_{\rm bq}) \exp\left(-\mathrm{HR}(\mathrm{SM})\cos^{\mathrm{NR\_P}}(\theta)\right) \tag{6}$$

where:

- Q is a **polarization coupling factor**, HR is a**n effective surface roughnes**s dimensionless parameter: HR $=$ $(2\ \mathrm{k}\ \sigma)^2$ where k is the wavenumber, σ is surface RMS height;
- $\mathrm{NR_p}$ is an integer used to parameterize the dependence of the roughness effects on incidence angle;
- $r_{\rm bq}$ designates the smooth surface reflectivity for alternate polarization.

Even though empirical, this formula has been tested in various occasions and found to work well, provided several precautions are taken. At L-Band, the main issues are related to the fact that soil roughness should rather be seen as a 1.4 GHz effective soil roughness, i.e., probably more related to the distribution of water in the top soil rather than a pure geometric soil surface roughness as the latter can only occur when the soil is very wet. Recent work indicates that HR is better modeled using shallower penetration depth at L-Band [47], but a moisture-dependent function [46], [48] was also tested with success and is currently implemented in the algorithm. For this, a soil water contribution is accounted for in HR. The principle is to have HR as a function of SM with a simple law. Below a transition moisture point, XMVT(C, S), the roughness is constant as well as above the field capacity, FC(C, S), where it takes the classical expression $(\mathrm{HR\_MIN(LC)} = (2\ \mathrm{k}\ \sigma)^2)$.

The HR value for dry soil can be set a priori and/or adjusted from the data. This formulation proved to be efficient but may still be questioned. As SMOS data are accumulated, we intend to see whether a better formulation (not using SM) could be found.

The two parameters XMVT and FC are function of the sand, S, and the clay, C, fractions.

From S and C, the transition moisture XMVT can be computed using the wilting point value. The value of $\mathrm{NR_p}$ is found to be between -2 and 2 from experimental data [49] Recent results indicated that the $\mathrm{NR_p}$ exponent is also polarization dependent. Polarization coupling effects are generally found to be rather weak at low frequencies. Therefore, it is often considered that $\mathrm{QR} = 0$ at L-Band and this value increases slightly with increasing frequency [49].

b) Effective soil temperature: The effective soil temperature $T_{\rm g}$ depends on the soil properties and moisture content profile within the soil volume. A simple formulation developed originally by [50] and then validated and revised [13], [51] is used in the algorithm. This formulation introduces two soil temperatures $T_{\rm soil\_surf}$ and $T_{\rm soil\_depth}$, to be selected from the four values supplied as auxiliary data (ECMWF fields).

The effective soil temperature is written as a function of the soil temperature at depth ($T_{\rm soil\_depth}$, approximately at 0.5 to 1m depth) and surface soil temperature ($T_{\rm soil\_surf}$, approximately between 1 and 5 cm) as follows [50]

$$T_{\rm g} = T_{\rm soil\_depth} + C_{\rm t}(T_{\rm soil\_surf} - T_{\rm soil\_depth}) \tag{7}$$

where $C_{\rm t}$ is a parameter depending mainly on frequency and SM. Wigneron *et al.* [49] computed $C_{\rm t}$ as a function of surface SM

$$C_{\rm t} = \min\left[(\mathrm{SM}/w_0)^{\mathrm{bw0}}, 1\right] \tag{8}$$

where the SM estimate SM is **taken from auxiliary data**; w_0 and b_{w0} are parameters that depend mainly on the soil texture and structure. To simplify, we will consider that

$$w_0 = \text{function}_\text{a}\ (\text{soil type})$$
$$\text{bw0} = \text{function}_\text{b}\ (\text{soil type}). \quad (9)$$

Obviously, for the global operational processor considered here, such pieces of information are not necessarily available nor really affecting the result as test done with the processor showed the limited impact (needless to say texture has significant effect on the emission though). We consider that the first layer and either the deepest or next to deepest layer given by ECMWF will give a good estimate of the surface and deep temperature. The errors induced are no more significant than those derived from using a crude interpolation scheme and have only impact in the case of very dry soils.

c) Low vegetation (grassland, crop): When a vegetation layer is present over the soil surface, it attenuates soil emission and adds its own contribution to the emitted radiation. At low frequencies, these effects can be well approximated by a simple model based on the RTE, hereafter referred to as the $\boldsymbol{\tau - \omega}$ **model**. This model is based on two parameters, the **optical depth** τ and the **single scattering albedo** ω, that are used to parameterize, respectively, the vegetation attenuation properties and the scattering effects within the canopy layer. The reflection at the top of the canopy (at the vegetation—atmosphere interface) is neglected.

No study could demonstrate the interest of using more complex radiative transfer models over rather low vegetation covers, where phase coherent effects (neglected by the RTE) may be significant [52]. Using the $\tau - \omega$ model [26], [52], global emission from the two-layer medium (soil and vegetation) is for each polarization p the sum of three terms: 1) the direct vegetation emission, 2) the vegetation emission reflected by the soil and attenuated by the canopy layer, and 3) soil emission attenuated by the canopy

$$\text{TB}_\text{P} = (1-\omega_\text{p})(1-\gamma_\text{p})(1+\gamma_\text{p} r_\text{gp}) T_\text{c} + (1-r_\text{gp})\gamma_\text{p} T_\text{g} \quad (10)$$

where T_g and T_c are the effective soil and vegetation temperatures, r_gp is the soil reflectivity, ω_p the single scattering albedo, γ_p the vegetation attenuation factor (where the c subscript has been dropped).

This last term can be computed from the optical depth τ_P as:

$$\gamma_\text{p} = \exp(-\tau_\text{p}/\cos\theta). \quad (11)$$

The above equation is a way to define a modified nadir optical depth $\tau_{0\text{p}}$ which is written as:

$$\tau_{0\text{p}} = \tau_\text{NAD} * \text{function}(\theta, p)$$

where the **nadir estimate of overall optical depth** $\boldsymbol{\tau_\text{NAD}}$ is independent of both incidence angle and polarization and the function (θ, p).

- **Surface temperature**: in most studies (forward modeling and retrievals), it is assumed that effective soil (T_g) and vegetation (T_c) temperatures are approximately equal to a single value $T_\text{gc} \approx T_\text{c} \approx T_\text{g}$. In particular, the effects of temperature gradients within the vegetation canopy should not be accounted for. With an overpass around dawn, the differences should be minimized and T_c can be expected to be close to the air temperature, while T_g can be estimated.

An estimate of an **effective** composite temperature T_gc (including **both** soil and vegetation media) could be roughly derived from the $\tau - \omega$ model and is given by the following equation:

$$T_\text{gc} = A_\text{t}\, T_\text{c} + (1 - A_\text{t}) T_\text{g} \quad (12)$$

With

$$A_\text{t} = B_\text{t}\,(1 - \exp(-\tau_\text{NAD}))$$
$$0 \le A_\text{t} \le 1.$$

The rationale of this equation is that as the vegetation biomass increases, both (i) attenuation of soil emission and (ii) vegetation emission increase, making the effective temperature closer to the vegetation effective temperature. Conversely, for bare soil conditions (i.e., for $\text{LAI} = 0$), T_gc is equal to T_g. When θ increases, T_gc becomes closer to the vegetation temperature as attenuation by the vegetation increases due to the $1/\cos(\theta)$ dependence. The dependence on incidence angle θ was not considered, simulations showing that this simplified equation remains accurate for most applications.

In equation, T_gc is assumed to be a linear function of T_c and T_g, and the weighting parameter A_t is assumed to depend on τ_NAD. The coefficient B_t used to compute A_t is assumed to depend on the canopy type. Simulations made with the $\tau - \omega$ model for a large range of values of optical depth, soil and vegetation temperatures, and incidence angles, provided an estimate of the default value of $B_\text{t} : B_\text{t} = 1.7$. As the temperature difference $(T_\text{gc} - T_\text{g})$ is small over low vegetation covers, we can use approximate τ_NAD values estimated from default values.

- **Scattering effects**: at L-Band, the value of the single scattering albedo ω is found to be rather low. For specific crop types (such as corn), ω can reach a value close to 0.1, but for most of low vegetation types, ω is lower than 0.05 and is neglected in most studies [53]. As the dependence of ω on θ could not be clearly demonstrated to date in the literature, it will be neglected in the algorithm. The value of ω will be given in the algorithm as a function of the vegetation type. The default value of ω, which was found to be valid over most types of crops will be $\omega_\text{V} = \omega_\text{H} = 0$ [53]. It is likely that the dependence of ω_P on polarization is rather low for most of low vegetation canopies.
- **Optical depth**: To model the optical depth τ_P, we propose accounting for the effects of the standing vegetation cover, litter, and water intercepted by the vegetation cover after rainfall or dew events as:

$$\tau_\text{P} = \tau_\text{SP} + \tau_\text{L} + \tau_\text{IP} \quad (13)$$

where $\tau_{\rm SP}$ is the optical depth of the standing vegetation cover, $\tau_{\rm L}$ is the optical depth of all the vegetation materials laying at the bottom of the canopy (including litter mainly), $\tau_{\rm IP}$ is used to parameterize the increase in optical depth due to intercepted water by the standing vegetation canopy (water intercepted by litter is included in the term $\tau_{\rm L}$). Note that, for the retrieval, we shall consider the nadir value $\tau_{\rm NAD}$ (i.e., for the incidence angle $\theta = 0$), including the contributions of the standing vegetation cover, litter and water intercepted by the vegetation cover. The accurate relationship between $\tau_{\rm p}$ and $\tau_{\rm NAD}$ is given in the following.

1) $\boldsymbol{\tau_{SP}}$ **is the optical depth of the standing vegetation cover** and includes both green and senescent vegetation materials.

Several studies found that $\tau_{\rm SP}$ could be linearly related to the total vegetation water content VWC (kg/m^2) using the so-called $b_{\rm P}$ parameter according to $\tau_{\rm p} = b_{\rm p}$ VWC [7]. At 1.4 GHz, a value of $b_{\rm P} = 0.12 +/- 0.03$ was found to be representative of most agricultural crops. However, it is very difficult to provide estimate of VWC at global scale. Also, recent studies found good correlation between $\tau_{\rm p}$ and vegetation indices (such as NDVI) or LAI.

Here, we propose to parameterize $\tau_{\rm SP}$ as a function of the LAI.

There are two main reasons for this: 1) it is much easier to build global maps of LAI from spaceborne remote sensing observations in the optical domain or from SVAT modeling with interactive vegetation [54] than maps of VWC; 2) several recent studies have also found good correlation between $\tau_{\rm SP}$ and LAI [21], [55] over a fallow; [11] over several crops [11] as first shown in [7].

The following equation is considered in LMEB:

$$\tau_{\rm SH}(\theta = 0) = \tau_{\rm SV}(\theta = 0) = \tau_{\rm S\_NAD} = b'_{\rm S}.{\rm LAI} + b''_{\rm S} \quad (14)$$

where the vegetation parameters $b'_{\rm S}$ and $b''_{\rm S}$ are function of the canopy type.

To compute optical depth $\tau_{\rm Sp}$, it is important to account for the effects of the vegetation structure: it was found that $\tau_{\rm Sp}$ depends on polarization and incidence angle, particularly for vegetation canopies with a dominant vertical structure (stem-dominated canopy such as cereal crops). Wigneron *et al.* [56] proposed a simple formulation using a polarization correction factor $C_{\rm pol}$ to parameterize this effect and compute the optical depth for cereal crops:

$$\tau\tau_{\rm H}(\theta) = \tau_{\rm NAD} \quad (15)$$

$$\tau\tau_{\rm V}(\theta) = \tau_{\rm NAD}\left[\cos^2\theta + C_{\rm pol}\sin^2\theta\right]. \quad (16)$$

Within a large-scale SMOS scene, it is likely that the effects due to the vegetation structure for a variety of vegetation types are averaged, so that the dependence of $\tau_{\rm p}$ on polarization and incidence angle can be neglected over most pixels. However, the possibility of accounting for this dependence should be kept in the algorithm to be used possibly over pixels with rather homogeneous vegetation cover. Thus, a generalization of these equations valid only for crops with a vertical structure has been developed.

Therefore, we chose to express $\tau_{\rm SV}(\theta)$ and $\tau_{\rm SH}(\theta)$ as a function of only one variable, namely $\tau_{\rm S\_NAD} = \tau_{\rm S}(\theta = 0)$, (which is estimated as a function of LAI, as defined above) according to:

$$\tau_{\rm SH}(\theta) = \tau_{\rm S\_NAD}\left(\sin^2(\theta).{\rm tt_H} + \cos^2(\theta)\right) \quad (17)$$

$$\tau_{\rm SV}(\theta) = \tau_{\rm S\_NAD}\left(\sin^2(\theta).{\rm tt_V} + \cos^2(\theta)\right) \quad (18)$$

where the ${\rm tt_V}$ and ${\rm tt_H}$ parameters are function of the canopy type and account for the dependence of $\tau_{\rm SP}$ on incidence angle.

These two equations are a generalization of the equation based on the polarization correction factor $C_{\rm pol}$ which was developed for vegetation with a vertical structure: applying $C_{\rm pol}$ to the standing vegetation optical depth $\tau_{\rm SP}$ corresponds to the particular case: ${\rm tt_H} = 1$ and ${\rm tt_V} = C_{\rm pol}$ ($C_{\rm pol} > 1$ for a vertical structure).

In the above equations we will thus neglect the dependence of $b'_{\rm S}$ and $b''_{\rm S}$S on 1) the canopy hydric status [57], [58] 2) the change of the vegetation structure in relation with phenology [24]. This dependence was shown to be relatively significant over crops, particularly during senescence, but it is likely that it has a low impact over large mixed pixels.

2) **Litter**:

Litter can be present in vegetation canopies, which are not (or rarely) ploughed: prairies or nonagricultural canopies, natural covers, forests, etc. Even though it is not well known, it is likely the effect of litter can be very significant in some cases [10], [21], [59], [60]... For instance, this effect was probably the implicit reason for using very high $b_{\rm P}$ values ($b_{\rm P} \approx 0.4$) over natural vegetation cover such as prairies. In L-MEB, litter is assimilated to a dense vegetation layer overlying the soil surface, characterized by the optical depth $\tau_{\rm L}$, assumed to be independent on incidence angle and polarization. A rather complex modeling approach in given in the SMOS ATBD and is not detailed here. This modeling is still not used currently as parameters have not been calibrated yet (studies are still in progress on these aspects). It is assumed, as for dew, that using the 2-Parameters approach (i.e., retrieving SM and TAU simultaneously), litter effects can be partly accounted for by increased values of the retrieved optical depth $\tau_{\rm \_NAD}$.

3) **Interception**:

$\tau_{\rm IP}$ is the optical depth that parameterizes the effect of **intercepted water** by the standing vegetation canopy, due to rainfall or dew events. Recent results have shown that these effects may be very significant: optical depth τ may increase by a factor of two or three during and after rainfalls over a fallow for instance.

Results obtained over a senescent wheat canopy showed that for moderate amount of intercepted water (less than 1.5-mm intercepted water), the L-Band measurements remained very sensitive to SM, and simultaneous retrievals of both SM and optical depth were possible [57]. An attempt to parameterize $\tau_{\rm IP}$, requiring estimations of the interception reservoir (mm) and of the fraction of intercepted water, depending on the

intensity of the rainfall events and of evaporation fluxes, would be very difficult.

Instead, it was decided to use an index **flagging** events during which interception effects are very significant (and during which it is very likely that SM cannot be retrieved). Preliminary results [55] showed that one of the best indices that can be used to flag interception at **local scale** is the **polarization ratio**$\mathrm{PR} = (\mathrm{TB_V} - \mathrm{TB_H})/(\mathrm{TB_V} + \mathrm{TB_H})$ at rather large incidence angle ($\theta \approx 50^\circ$). Significant interception events are associated to **low** values of PR.

In summary, the vegetation type and the LAI (characterizing the vegetation phenological stage and thus indirectly the vegetation structure) are the main parameters determining the values of the parameters used in the $\boldsymbol{\tau - \omega}$ **model**: $b', b''_{\mathrm{S}}, \mathrm{tt_V}, \mathrm{tt_H}$, ω and the intensity of specific effects such as litter and interception.

2) Forests: A large fraction of land is covered by forests. All efforts aimed at fully exploiting the potential of SMOS over these areas must be done. The attenuation due to crown and litter is strong, as confirmed by some experiments [59], [60]. However, an appreciable, although limited, sensitivity to SM variations was observed in forests not too dense and with a thin litter [61]–[63].

A pure empirical approach, based on τ and ω parameters fitted over experimental data is not appropriate to forests, because presently available radiometric measurements are limited. Moreover, multiple scattering effects are appreciable and the application of a simple first-order approach is not straightforward.

In any case, the methodology adopted for forests was harmonized with the general SMOS SM retrieval algorithm, and the complexity of the operational procedure was kept limited. The adopted approach is summarized below (details are available in [64]).

- The simple first-order formulas based on "albedo" and "optical depth" are kept.
- From land cover classes, three forest categories are aggregated: needle leaf, broadleaf (including tropical forests and woodland), mixed forest. The same general procedure is applied for the three categories, although the output parameters are specific of each single category.
- The values of albedo and optical depth are assigned by a preliminary modeling work based on the software already available at Tor Vergata University, with suitable refinements and adaptation to specific cases [65]–[68]. The output of this basic direct modeling work consists of look-up tables, relating sets of simulated emissivities (for the SMOS configuration) to SM, for the three forest types indicated above. Using allometric equations available in the literature for the different forest categories, geometrical and biophysical inputs required by the model are related to LAI_{Fmax}, (maximum yearly value of arboreous LAI). For an elementary surface of forest, LAI_{Fmax} is used to compute the contribution of all arboreous components (tree trunks, branches, and leaves in maximum development) to the total optical thickness, while LAI_V (LAI due to herbaceous vegetation) is used for the time dependent contribution of low vegetation understory to this total optical thickness [64], [66], [67]. These two quantities, which are available by ECOCLIMAP, partition the total forest optical thickness into two contributions and do not represent absolute LAI's but fractional LAI's.

Then, a standard RMS minimization routine is used to find the equivalent values of the parameters (optical depth and albedo) to be assigned to a simple first-order model, like the one adopted for low vegetation, in order to behave most similarly to the discrete multiple scattering model. This RMS minimization is made by considering, for each forest scenario, several sets of angles and SM values. This operation is named **parameterization**. Details are given in [64] and [69]. The output produced after this step consists in estimating the albedo and relating the nadir optical depth to LAI_{Fmax}, and LAI_V, with coefficients depending on forest type. These two **forest** parameters (**equivalent** nadir optical depth and albedo) are indicated by τ_{F_NAD} and ω_F, respectively. It is found in [64] that, due to the wide range of orientation angles of branches and leaves, $\tau_{\mathrm{F\_NAD}}$ and ω_{F} can be assumed to be independent on polarization.

- With the two values obtained by the previously described parameterization, the successive algorithm steps are similar to the low vegetation case. The basic formulas of Section IV-C1 are used also for forests, leading to a unified approach. In particular, a simple formula is used to compute the nadir equivalent optical depth τ_{FNAD}, such as:

$$\tau_{\mathrm{F\_NAD}} = \tau_{\mathrm{FA}} + b_{\mathrm{V}}.\mathrm{LAI_V} \tag{19}$$

where:

$$\tau_{\mathrm{FA}} = b'_{\mathrm{F}}\mathrm{LAI_{Fmax}}. \tag{20}$$

b'_F, and b_V values, specific of the forest categories, are obtained as a result of the parameterization. It is also assumed that ω_F does not depend on LAI_{Fmax}.

The TB may be finally computed as:

$$\mathrm{TB_p} = (1-\omega_{\mathrm{F}})(1-\gamma)(1+\gamma r_{\mathrm{gp}})T_{\mathrm{c}} + (1-r_{\mathrm{gp}})\gamma T_{\mathrm{g}} \tag{21}$$

where T_g and T_c are the effective soil and vegetation temperatures, r_{gp} is the soil reflectivity, ω_F is the equivalent albedo, and γ is the vegetation transmissivity, given by:

$$\gamma = \exp(-\tau_{\mathrm{F\_NAD}}/\cos\theta). \tag{22}$$

As previously stated, the basic algorithm for forests is similar to the one used for low vegetation. The main differences are listed below:

- A simple τ_{F_NAD} constant, without correcting factors depending on polarization and angle, may be used in (22). This is a result of the variability in orientation of branches and leaves.
- ω_{F} may be considered constant (i.e., independent on angle, polarization and time). However, it is **not** negligible, since its value is 0.08 (see [62], [64]).

τ_{F_NAD} includes contributions due to crown, litter and under storey [66], [67]. The contribution of litter is computed using the model of [70], which considers the litter as a continuous layer overlying the soil [70]. Its thickness is related to the same LAI_{Fmax} static parameter, while litter permittivity is estimated by assuming a given ratio between SM and litter moisture [70]. The procedure is subdivided into these steps: 1) Compute the permittivity of the soil; 2) Compute the permittivity of the litter as a function of SM, dry weight matter density, and assumed ratio between SM and litter moisture; 3) estimate litter layer thickness as a function of LAI_{Fmax} and vegetation type; 4) using simple formulas given in [69], compute the reflectivity of the ensemble soil+litter for flat interface; 5) apply roughness correction.

3) Other Surface Types:

a) Dry sand: In itself, sand is simply a soil type and could be considered as a purely nominal case. However, due to its own characteristics, it has almost no bound water and hence has specific dielectric constant behavior. Moreover, sand has specific water capacities and can be very dry, leading to large penetration depths. Hence, the usual equations are bound to be less and less accurate as sand proportion increases and should be corrected.

It is often considered that the dielectric constant of sand can be expressed at 1.4 GHz [71]:

$$\varepsilon_{\mathrm{dry-sand}} \approx 2.53 - 0.05j. \tag{23}$$

A specific model might be developed from this expression. However, since it is not currently available, in the mean time the one given using Dobson's model [39], [40] with the Peplinsky formulation [72], [73] was used for sandy areas. It is going to be replaced by the Mironov model [41]–[43].

b) Open water: Most land surfaces include extended water surfaces, which may be the ocean for coastal pixels, or inland features such as rivers, canals, lakes, ponds, flooding, etc. To derive a sensible value for SM, these contributions have to be taken into account.

The emission by water bodies is estimated by assuming the validity of the Fresnel equations and deriving the dielectric constant of an assumed flat water body

The **real** (dominant) and imaginary parts of the complex dielectric constant for free water $\varepsilon_{\mathrm{w}} = \varepsilon'_{\mathrm{w}} - j\varepsilon''_{\mathrm{w}}$ at a given radiometer frequency f are given by the modified Debye equation [74]. For **saline water** with a salinity S, the static dielectric constant of water, ε_{sw0}, is derived using [75] and the relaxation time of saline water, $\mathbf{r}\tau_{sw}$, is given by Stogryn [76].

c) Very dry soils, rocky out crops, and other specific surfaces: Very dry soils do have a specific behavior linked to the different roles of bounded versus free water. To account for this, we can adapt the dielectric model with one caveat, that is such models (Wang for instance) show a discontinuity in the derivative which may pose problems. Otherwise, very dry soil might exhibit extreme penetration depth and thus complicate the estimation of the equivalent temperature. As very dry soils are usually 1) without vegetation, 2) of little interest for water fluxes, we believe this specific case should only be of concern for very limited cases.

d) Rocks and rocky out crops: Rocks and rocky areas are not well modeled for the time being and generally assumed to behave as very dry soils. Field measurements do not show significant effects from rocks [77]. It is also worth noting that rocks and the like are usually on barren areas or in mountains, etc. . . and thus of concern for only a limited number of cases. Effectively, problems may arise only when a significant amount of surface is covered with rocks (boulders, steep high mountains, cliffs), or when the dry soils or rocky outcrops have very specific signatures. In all those latter cases, the issue will only complicate existing issues and such cases will probably have to be flagged and the algorithm directed toward dielectric constant values estimation.

In [74], permittivity values are given for rocks at 400 MHz and 35 GHz. They range from 2.4 to 9.6. Approximate expressions do exist (see Weiner's model for powdered rocks for instance) for rocks, but it does not seem worth the effort to implement in the level 2 algorithm for the reasons given above. The retrieval algorithm considers

$$\varepsilon_{\mathrm{rock}} = 5.7 - j * 0.074. \tag{24}$$

e) Other specific soil surface cases: In some instances, the surface will be affected by other factors such as mineral deposits, salted residues (salt lakes for instance), or surface with very specific dielectric constants.

With current knowledge, this can only be addressed with the dielectric approach. Below 10 GHz, the ionic conductivity of saline water has a marked effect on the loss factor and this is used in SMOS for salinity retrievals. However, the exact form of the dependence of the dielectric constant on soil salinity is not well understood, due to the very sparse measurements available.

4) Urban: Urban areas are the most complex due to the varying mix of earth vegetation areas, with buildings (i.e., similar to rock or earth depending on the material used for roofing when old and metallic in new commercial—warehouses industrial areas) more over the structure are organized in space with geometrical shapes. And finally, roads (sometimes with trees) and RFI might also influence the signal.

However, this is still a placeholder. Models are not yet available for cities, so they are assumed to behave as **barren soil** for a start, and the surface assumed to be similar to rocks. As much as possible, the concerned areas will be restricted to dense urban areas (including airports), while more sparsely populated suburbs are considered as vegetated regions.

5) Topography: The process of retrieving SM and vegetation opacity relies on the use of angular signatures. Obviously, it is necessary to have a reference angle, and an inclined surface may behave quite differently as a function of azimuth viewing wrt to the same but "horizontal" surface. At SMOS scales, we will never encounter such inclined surfaces, but the pixel, when corresponding to a mountainous area, will present various facets of varying slopes and azimuths inducing effects which may eventually render the inversion impossible. Added to this, are the shadowing and adjacency effects.

Two previous studies [19], [78] tried to cover the point of topography, and currently it seems that up to a certain level, the almost ever present topography can be totally neglected

(gently rolling hills), to premountains. There is then a range of topography characteristics for which the algorithms should be able to retrieve some values but with larger error bars or little significance (old and eroded mountains, mountains with plateaus, etc...). It corresponds to what we call "soft topography."

Finally, very rugged mountains (strong topography) will cause the signal to be useless. The approach relies on provided a topography index [20] which is then used to flag mountainous areas as per their topography.

a) Rivers: Vector rivers data are available from ESRI's "Digital Chart of the World" data set [79].

For most rivers, there is no associated width, and indeed any estimated width would be subject to local weather and tidal conditions; however wide rivers are coded as lakes with an associated area, and in these cases, the vector data can be converted to raster to generate open water area estimates.

6) Time-Dependent Surfaces:

a) Water bodies: Abnormal retrieval in some areas may allow flooding conditions to be flagged, if other conditions can be discounted. Potential confounding environmental conditions include:

- The seasonal behavior of large rivers.
- The presence of very flat beaches, which give rise to highly variable areas of water coverage.
- Large rain events causing significant ponding.
- Areas of extended gravimetric irrigation and/or rice growing areas...etc. Finally, and this might turn out to be an application area, wetlands will pose specific but related issues.

While some water bodies are rather stable with time, others do fluctuate significantly (some rivers (e.g., Niger) due to the rainfall pattern or other factors (e.g., freezing for the Ob). Some lakes are stable in dimension; others fluctuate with season (e.g., Chad Lake). To go to the extreme, estuaries fluctuate as well (tidal effects) as well as deltas (Okavango). This may have a significant impact and cannot be addressed with a fixed inland water/land map. It may be noted that ECOCLIMAP flags tidal flats.

Coastal pixels might induce some errors (variable water/wet sand/dry sand limits). This point is not currently covered in the algorithm. Similarly flooding (area which are regularly or seasonally flooded (not the special events) are considered here) will have an impact.

To correctly take into account water bodies, an evolving water/land mask is necessary, which has yet to be found or established. There might be possibilities with MODIS data but this will have to be addressed. The fall back option is to identify areas prone to such events and flag them.

Pending further developments, a flood flag is set depending on the amount of past local rain.

b) Frozen soils and ice: Frozen soils cover large areas at high latitudes (and sometimes altitudes). At mid latitude, frozen soil can also be expected in winter, particularly for the morning orbit. Experience shows that the dielectric properties of frozen soil are very close to those of dry soil, while vegetation is almost fully transparent [16]. It is often considered that for frozen soils the dielectric constant can be written [15]:

$$\varepsilon_{\mathrm{frz}} = 5 - 0.5\mathbf{j}. \tag{25}$$

The algorithm thus delivers a "dry bare soil" output when soil is frozen. The presence of frozen soil is identified by this "very dry bare soil" result from the retrieval when other variables such as air temperature, vegetation cover, and retrieved soil temperature are consistent. It should also be borne in mind that frozen ground often shows extreme spatial heterogeneity, complicating the matter.

The areas of **permanent** ice/dry snow are known, and will be masked out, so that only the dielectric constant is retrieved. (e.g., Greenland, Antarctica...). For other areas or partial ice (mountains, cold lakes), the idea is that above a given threshold the dielectric constant could be retrieved.

It can be noted however that ice is rather transparent, with $\varepsilon''_{\mathrm{ice}}$ being very small ($\varepsilon''_{\mathrm{ice}} = 0.1$ in [80] for pure ice) as given in [17]:

$$\varepsilon_{\mathrm{ice}} \approx 3.17 - \mathbf{j}\varepsilon''_{\mathrm{ice}}. \tag{26}$$

c) Snow: Snow covers up to about 40% of the Northern hemisphere land mass seasonally, but has very different dielectric properties depending on its history. Fresh, dry snow is transparent to microwave radiation; however, as snow melts its dielectric constant increases dependent upon snow grain size and liquid water content and may be totally opaque (at $T_e \cong 273$ K) when wet. Consequently, the effects of snow are too complicated to be incorporated into the currently proposed algorithm, and areas with significant snow coverage other than dry snow must be considered as retrievable only in terms of an equivalent dielectric constant. The issue will be in identifying and flagging the snow covered areas. For this purpose, in the current version of the algorithm, the information is obtained from ECMWF forecasts which give the information on snow presence and temperature. The main caveat is that the spatial resolution is much coarser than the required one $(0.25 \times 0.25^{\circ})$. As a consequence, the ECMWF percentage of snow cover is distributed on the most northern DFFG under consideration. This is very coarse so the goal is to implement the Interactive Multi satellite Snow and Ice System [81].

D. The Cardioid Model

In the cases of vegetated soil as well as open water, the basis of physical modeling consists of writing the reflectivity (or emissivity) for a smooth surface as a function of the complex dielectric constant $\varepsilon = \varepsilon' - j\varepsilon''$. In turn, the dielectric constant is written as a function of physical parameters, including surface SM for the vegetated soil or salinity for open water. For cases where ε cannot be expressed in the same way (e.g., iced surfaces), it is still possible to retrieve, from SMOS data, information about the dielectric constant. It has been shown [82] that, to a very good approximation, ε can be written:

$$\begin{aligned} \varepsilon' &= \mathrm{A\_card}\,(1 + \cos(\mathrm{U\_card}))\cos(\mathrm{U\_card}) + \mathrm{B\_card} \\ \varepsilon'' &= \mathrm{A\_card}\,(1 + \cos(\mathrm{U\_card}))\sin(\mathrm{U\_card}). \end{aligned} \tag{27}$$

When A_card is constant, this is the parameterized expression for a function that reduces to a cardioid when B_card is taken equal to 0. Hence, the name of "modified cardioid."

Or conversely:

$$\begin{aligned} \text{A\_card} &= \text{m\_card}2/(\text{m\_card} + \varepsilon' - \text{B\_card}) \\ \text{U\_card} &= \tan -1\,(\varepsilon''/(\varepsilon' - \text{B\_card})) \end{aligned} \tag{28}$$

with: $\text{m\_card} = ((\varepsilon' - \text{B\_card})2 + \varepsilon''2)1/2$

The optimal value for B_card is very close to 0.8.

It turns out that these expressions are relevant because angular-dependent radiometric data allow retrieving accurately the value of the magnitude A_card, while, on the other hand, the retrieval accuracy on the polar angle U_card is extremely poor; indeed, the emissivity is almost independent of U_card, to the extent that almost any a priori value can be stipulated for the angle U_card. In this situation, while retrieving both ε' and ε'' would result in very large uncertainties, the modified cardioid approach can be understood as a regularisation of the retrieval problem. Therefore, in cases considered above, SMOS data can still be used to derive an estimate for the magnitude A_card, which will be referred to as the dielectric constant index.

This may be useful, as any additional independent information on the dielectric constant might then be used to infer the full complex ε. For the cases of vegetated soil or open water, values for A_card and U_card may be computed readily from the complex dielectric constant (which is available using the retrieval when retrieved values for SM or SSS are introduced in the direct model), using the above equations, if necessary. They can then be used as initial values in case a complementary retrieval using the modified cardioid formulation is attempted.

This model is a particular case in the sense that its implementation is not completely identical depending whether it is used for direct simulation or retrieval.

E. Other Contributions to the Radiometric Signal

Corrective terms in the RTE refer to ionospheric (Faraday) rotation and sky and atmospheric contributions. Faraday rotation is taken care of in the geometrical transformation from antenna to TOA. The atmospheric contribution is derived from [26] and parameterized as in [83] to enhance speed. Other unwanted contributions are the RFI [84]. The retrieval algorithm identifies RFI either through abnormally high or low values as well as unexpected angular behavior.

Those outliers are suppressed before the retrieval process begins but may lead to very few angles left and hence make retrieval either very poor or not possible.

V. Results and Discussion

Results are available elsewhere in this SMOS Special Issue so it does not seem necessary to delve too much on them here. We can only state that globally the retrieval algorithm performs well in terms of coverage with the big caveat of the RFI which affect Europe and Asia mainly. Although this should be qualified since possible errors such as those due to default contributions are not included, the quality of the results is almost within expectations (0.04 m3/m3) which is encouraging when you consider that the satellite has been operating for only two years. Good results are obtained over RFI free low vegetation and encouraging results over moderately dense forests [85]. What needs to be tackled in the near future is the vegetation opacity retrieval which is not always behaving as expected. The values do oscillate a lot and do not always follow the expected seasonal cycle. There could be several causes to this problem such as: modeling errors, poor parameterization, poor angular intercalibration of the instrument etc... Another explanation could that opacity is not as simple as we would like it to be. Only detailed analysis of results will enable to make progresses on this point.

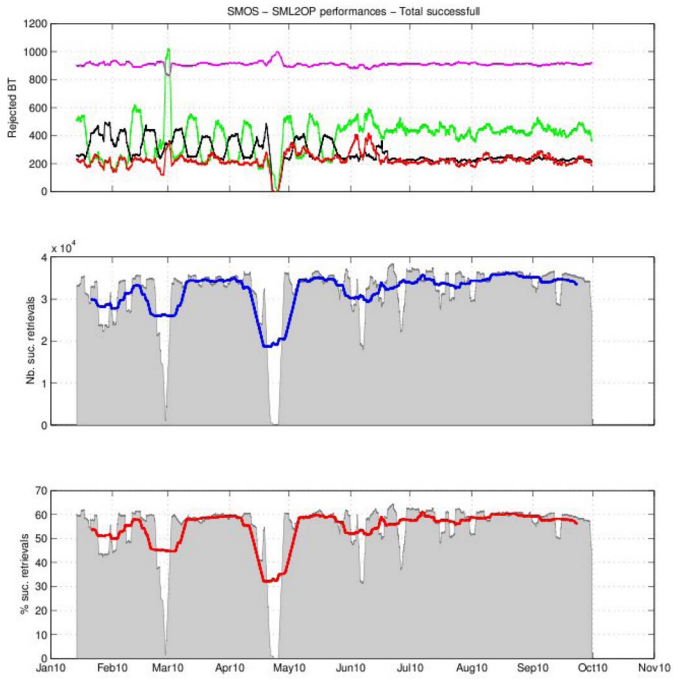

Fig. 4. Overall statistics of the retrievals for year 2010. The top panel gives the number of points available for retrievals the middle the number of successful retrievals and the lower the percentage of success. The shaded part corresponds to a running average over 3 days and the blue line over 18 days. In the top panel, the colors correspond to magenta: points discarded because the spatial resolution was to coarse, green discarded due to too high a brightness temperature, black: anomalous angular behavior, red: the signal amplitude is too large.

Globally SM retrievals are in the right range of values with a general tendency to underestimate ground measurements. The underestimation is strongly increased by RFI as could be expected. However, in some cases and after a heavy rainfall event, the obtained SM values seem too high (sometimes exceeding 0.65 m3/m3). This may be due to ponding effects, saturation of the upper soil layer, or retrieval errors.

Another point of concern is the way cold areas are processed. If freeze thaw is easily detected (soil appears suddenly dry when it freezes and vegetation becomes transparent when frozen). The main issue at this level is the fact that a high spatial resolution is required to monitor freeze thaw, particularly in the transition areas. Snow cover is more complex. When dry, snow is almost transparent, and SMOS is sensitive to the relatively warm soil underneath. However, when the snow is wet, it is rather opaque. All the intermediary cases (both in term of

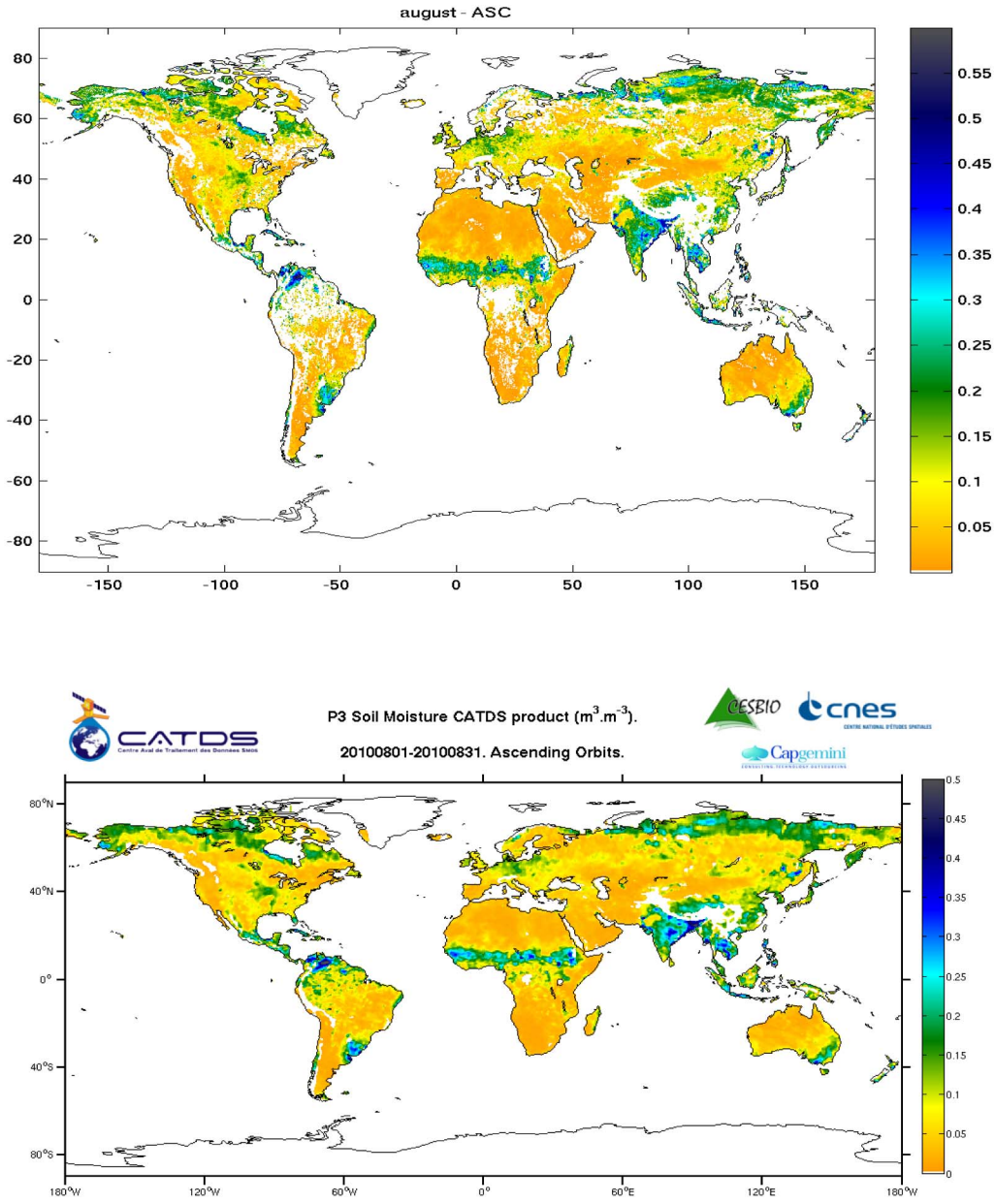

Fig. 5. Global map of soil moisture derived from SMOS data for the month of August 2010. Top panel 3 day composite, bottom panel monthly composite/color scale is soil moisture expressed in m^3/m^3.

snow state and spatial distribution), make retrieval in transition areas very difficult and the product is prone to be erroneous. Another source of concern is linked to water bodies. There are no available dynamic maps of water bodies at a fine enough resolution. And water bodies do change with time, be it through seasonal variations, floods or even tides. An error of 2% on the water body surface can lead to an error in SM corresponding to 0.01 m3/m3.

The evaluation of the retrieval algorithm has been going on since the onset of the commissioning phase. Most of the algorithm evaluation is presented in this issue. At first, all the efforts were concentrated in the Australian area where an extensive campaign (AACES for Australian Airborne Cal Val Experiment for SMOS [86], [87]) took place. It was then the main area with active vegetation (it was winter in the Northern Hemisphere), with the added advantages of being practically RFI free while an intensive airborne campaign was taking place. After, the focus shifted to other areas such as Africa (Niger and Benin), the watershed sites in the US, the various Cal-Val sites in Europe, and the SCAN sites. See this issue for details on all these campaigns and related results.

The overall performances of the algorithm were established by first looking at the overall statistics as shown in Fig. 4.

One can see that overall the algorithm performs reasonably well except for the commissioning phase period when the instrument was tuned and tested extensively, giving way to data losses. In early May 2010, there was an electrical stability test for instance which resulted in one week without data. This figure also shows that there is room for improvement as, even considering factors such as RFI, topography or any other

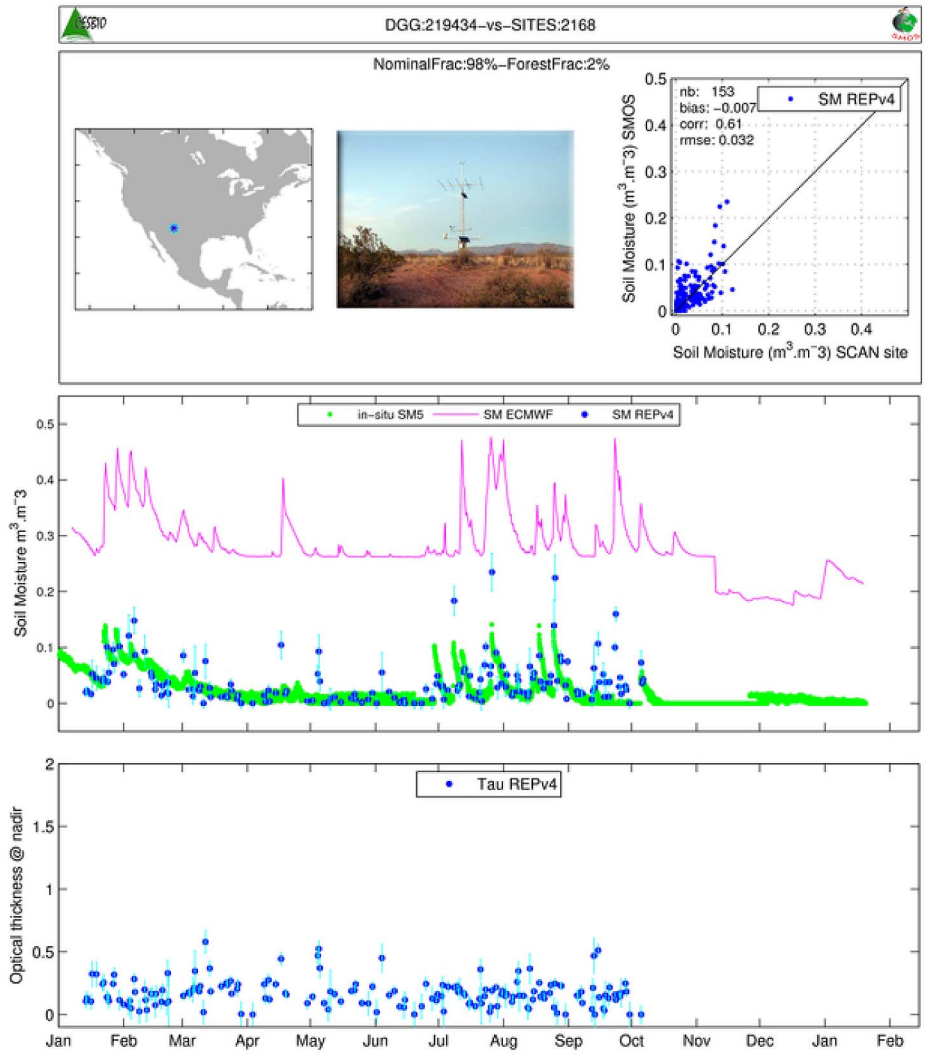

Fig. 6. Performances of the algorithm on a ground site (SCAN network) the top panel gives the location of the site, a photograph of it and the scatter plot (ground versus SMOS). The middle panel gives the SMOS data (blue dots) together with the ground measurements (green line) and the ECMWF estimates (magenta line) the abrupt change on November 9, 2010 is linked to a model update at ECMWF).

perturbation, the average success rate is only slightly higher than 60%.

This can be seen again on Fig. 5 where the top panel gives an overview of a three-day composite (i.e., global coverage) using only ascending passes. There are many gaps explained by the lack of successful retrievals: RFI in many cases, erroneous retrievals, or areas where SM retrievals were not attempted (high topography index, permanent snow, and ice, etc. . .;)

The bottom panel shows that when data are accumulated over a month, it is possible to achieve a much better coverage.

Another way to estimate retrieval quality is to compare the data to ground measurements as shown on Fig. 6. For this site located in SW US results are also rather satisfactory. Of course, some areas do not behave so well with many cases showing a higher correlation (partly due to a larger range of SM values) but also a RMSE exceeding the 0.04 m3/m3 target.

It is also well known that sites are not necessarily representative of a SMOS like pixel, explaining some poor comparison results obtained in some cases (heterogeneous areas for instance).

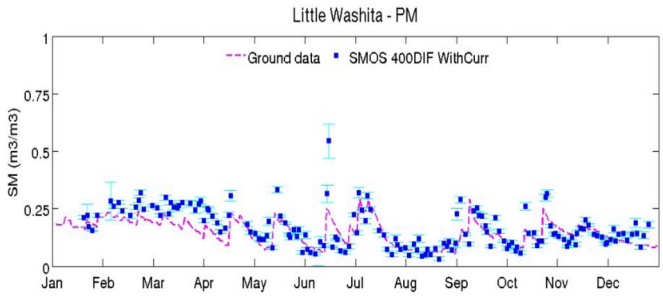

Fig. 7. Results obtained over a site where the ground data were averaged over an area to be comparable with satellite data. The site is the Little Washita watershed in Oklahoma. Blue dots correspond to SMOS measurements (descending pass) and magenta line to averaged soil moisture.

To check this point, data were also compared to area averaged data obtained by merging several ground measurements [88]. Fig. 7 shows the results obtained when SMOS data is compared to the Little Washita Site (descending orbits in this case. One

can see that SMOS compares quite well with the spatially average data.

Quantitative evaluation of the L2 algorithm is described in several papers of this issue as well as in other publications. Globally, the results are very satisfying for the low vegetation cases in areas not too much affected by RFI such as in the US or Australia. Conversely, in Europe, for instance, results so far are degraded. Results are mediocre over forested areas currently but intensive research is being carried to understand better the reasons why. Over arid areas the results are very good. From the range of results obtained, one can say that roughly depending on area and RFI levels, the SM estimates accuracy range between 0.02 and 0.06 m^3/m^3 with, in some cases, even higher values, while correlations between ground measurements can range from 0.5 to 0.85. More details on specific cases can be found in papers in this special issue. Several studies also compared SMOS retrievals to other sensors' retrievals. Usually, SMOS fares very well particularly when considering that it is a new sensor while the other have much longer track records.

VI. Conclusion

SMOS was a new approach to new measurements. After a year in operation and 1.5 year in orbit, the results are outstanding. For SM, one of the main goals of the mission, results are very promising. They are still not to where they are expected to be but are already quite good for the simplest targets homogeneous low vegetation, as shown in [89]. Good results are also starting to emerge over forested areas.

The challenge to build before launch a retrieval algorithm with experience of neither L-Band measurements, nor synthetic aperture radiometer or even SM, proved to be successfully taken up as, even though still in infancy, the combination of satellite and retrieval algorithm gave results immediately after switch on. The option taken (iterative Bayesian and physically based models) proved to be satisfactory. The main issue encountered was the RFI pollution, but things are improving in this domain as well [84], [90].

Now, the challenge will be to have the retrieval being first more accurate and second over more and more surface type. Another goal is to develop and make full use of the cardioid estimates of the dielectric constant.

In parallel, investigating statistical approaches will be initiated now that some insight of SM at 40-km spatial resolution is available.

Acknowledgment

The authors are greatly indebted to the scientists who in the 70s and the 80s did all the ground work enabling the SMOS project. We are also indebted to the SMOS Project and Mission Managers as well as to the Level 1 team for their continuous collaboration, in particular the ESA ESAC team. Contributions from all the Ground Teams are also highly appreciated, and we are in particular very thankful to Jeff Walker, Christoph Rudiger and the Monash University team as well as Tom Jackson and the USDA ARS team.

References

[1] T. J. Schmugge, "Applications of passive microwave observations of surface soil moisture," *J. Hydrol.*, vol. 212/213, pp. 188–197, Dec. 1998.

[2] T. J. Schmugge and T. J. Jackson, "Mapping soil moisture with microwave radiometers," *Meteorol. Atmos. Phys.*, vol. 54, no. 1–4, pp. 213–223, Mar. 1994.

[3] W. Wagner, G. Bloschl, P. Pampaloni, J. C. Calvet, B. Bizzarri, J. P. Wigneron, and Y. Kerr, "Operational readiness of microwave remote sensing of soil moisture for hydrologic applications," *Nordic Hydrol.*, vol. 38, no. 1, pp. 1–20, 2007.

[4] Y. H. Kerr, "Soil moisture from Space: Where are we?" *Hydrogeol. J.*, vol. 15, no. 1, pp. 117–120, Feb. 2007.

[5] Y. Kerr, P. Waldteufel, P. Richaume, I. Davenport, P. Ferrazzoli, J.-P. Wigneron, SMOS Level 2 Processor Soil Moisture ATBD, SM-ESL (CBSA), Toulouse SO-TN-ESL-SM-GS-0001, 24/10/2010, 2010.

[6] B. K. Hornbuckle and A. W. England, "Vegetation canopy anisotropy at 1.4 GHz," in *Proc. IGARSS*, Toulouse, France, 2003, pp. 333–335.

[7] T. J. Jackson and T. J. Schmugge, "Vegetation effects on the microwave emission of soils," *Remote Sens. Environ.*, vol. 36, no. 3, pp. 203–212, Jun. 1991.

[8] C. Matzler, "Microwave transmissivity of a forest canopy—Experiments made with a beech," *Remote Sens. Environ.*, vol. 48, no. 2, pp. 172–180, May 1994.

[9] E. G. Njoku and L. Li, "Retrieval of land surface parameters using passive microwave measurements at 6-18 GHz," *IEEE Trans. Geosci. Remote Sens.*, vol. 37, no. 1, pp. 79–93, Jan. 1999.

[10] J. P. Grant, K. Saleh, J.-P. Wigneron, M. Guglielmetti, Y. Kerr, M. Schwank, N. Skou, and A. A. Van de Griend, "Calibration of the L-MEB model over a coniferous and a deciduous forest," *IEEE Geosci. Remote Sens.*, vol. 46, no. 3, pp. 808–818, Mar. 2008.

[11] J.-P. Wigneron, Y. Kerr, P. Waldteufel, K. Saleh, M.-J. Escorihuela, P. Richaume, P. Ferrazzoli, J. P. Grant, B. Hornbuckle, P. de Rosnay, J.-C. Calvet, T. Pellarin, R. Gurney, and C. Mätzler, "L-band microwave emission of the biosphere (L-MEB) model: Results from calibration against experimental data sets over crop fields," *Remote Sens. Environ.*, vol. 107, no. 4, pp. 639–655, Apr. 2007.

[12] D. Entekhabi, I. Rodriguez-Iturbe, and F. Castelli, "Mutual interaction of soil moisture state and atmospheric processes," *J. Hydrol.*, vol. 184, no. 1/2, pp. 3–17, Oct. 1, 1996.

[13] T. R. H. Holmes, P. de Rosnay, R. de Jeu, J.-P. Wigneron, Y. H. Kerr, J.-C. Calvet, M. J. Escorihuela, K. Saleh, and F. Lemaitre, "A new parameterization of the effective temperature for L-band radiometry," *Geophys. Res. Lett.*, vol. 33, p. L07 405, Apr. 2006.

[14] R. L. Armstrong and M. J. Brodzik, "Recent northern hemisphere snow extent: A comparison of data derived from visible and microwave sensors," *Geophys. Res. Lett.*, vol. 28, no. 19, pp. 3673–3676, 2001.

[15] M. T. Hallikainen, "Retrieval of snow water equivalent from NIMBUS-7 SMMR data—Effect of land-cover categories and weather conditions," *IEEE J. Ocean. Eng.*, vol. OE-9, no. 5, pp. 372–376, Dec. 1984.

[16] C. Matzler, "Passive microwave signatures of landscapes in winter," *Meteorol. Atmos. Phys.*, vol. 54, no. 1–4, pp. 241–260, Mar. 1994.

[17] C. Matzler and U. Wegmuller, "Dielectric-properties of fresh-water ice at microwave-frequencies," *J. Phys. D, Appl. Phys.*, vol. 20, no. 12, pp. 1623–1630, Dec. 14, 1987.

[18] T. Pellarin, Y. H. Kerr, and J. P. Wigneron, "Global simulation of brightness temperatures at 6.6 and 10.7 GHz over land based on SMMR data set analysis," *IEEE Trans. Geosci. Remote Sens.*, vol. 44, no. 9, pp. 2492–2505, Sep. 2006.

[19] C. Matzler and A. Standley, "Relief effects for passive microwave remote sensing," *Int. J. Remote Sens.*, vol. 21, no. 12, pp. 2403–2412, Aug. 2000.

[20] A. Mialon, L. Coret, Y. H. Kerr, F. Sécherre, and J.-P. Wigneron, "Flagging the topographic impact on the SMOS signal," *IEEE Geosci. Remote Sens.*, vol. 46, no. 3, pp. 689–694, Mar. 2008.

[21] K. Saleh, J.-P. Wigneron, P. de Rosnay, J.-C. Calvet, and Y. Kerr, "Semi-empirical regressions at L-band applied to surface soil moisture retrievals over grass," *Remote Sens. Environ.*, vol. 101, no. 3, pp. 415–426, Apr. 2006.

[22] K. Saleh, J.-P. Wigneron, P. Waldteufel, P. de Rosnay, M. Schwank, J.-C. Calvet, and Y. H. Kerr, "Estimates of surface soil moisture under grass covers using L-band radiometry," *Remote Sens. Environ.*, vol. 109, no. 1, pp. 42–53, Jul. 2007.

[23] J. P. Wigneron, Y. Kerr, and L. Prévot, "Retrieval of soil and vegetation features from passive microwave measurements," *Remote Sens. Rev.*, vol. 15, no. 1–4, pp. 157–177, 1997.

[24] J.-P. Wigneron, J.-C. Calvet, P. de Rosnay, Y. Kerr, P. Waldteufel, K. Saleh, M. J. Escorihuela, and A. Kruszewski, "Soil moisture retrievals from biangular L-band passive microwave observations," *IEEE Geosci. Remote Sens. Lett.*, vol. 1, no. 4, pp. 277–281, Oct. 2004.

[25] J. Shi, L. M. Jiang, L. X. Zhang, K. S. Chen, J.-P. Wigneron, and A. Chanzy, "A parameterized multi-frequency-polarization surface emission model," *IEEE Trans. Geosci. Remote Sens.*, vol. 43, no. 12, pp. 2831–2841, Dec. 2005.

[26] Y. H. Kerr and E. G. Njoku, "A semiempirical model for interpreting microwave emission from semiarid land surfaces as seen from space," *IEEE Trans. Geosci. Remote Sens.*, vol. 28, no. 3, pp. 384–393, May 1990.

[27] Y. H. Kerr, RAMSES: Proposition de Mission Spatiale sur Mini satellite au Colloque de Prospective du CNES (TAOB)1997, CESBIO, Toulouse, Proposal November 1997.

[28] Y. H. Kerr, The SMOS Mission: MIRAS on RAMSES. A Proposal to the Call for Earth Explorer Opportunity Mission1998, CESBIO, Toulouse (F), Proposal 30/11/1998.

[29] G. Lagerloef, J. Font, C. Koblinsky, and R. Colomb, "The aquarius/SAC-D salinity mapping mission and synergies with SMOS," in *Proc. IEEE IGARSS*, Toulouse, France, 2003.

[30] D. Entekhabi, E. G. Njoku, P. Houser, M. Spencer, T. Doiron, Y. J. Kim, J. Smith, R. Girard, S. Belair, W. Crow, T. J. Jackson, Y. H. Kerr, J. S. Kimball, R. Koster, K. C. McDonald, P. E. O'Neill, T. Pultz, S. W. Running, J. C. Shi, E. Wood, and J. van Zyl, "The hydrosphere state (Hydros) satellite mission: An earth system pathfinder for global mapping of soil moisture and land freeze/thaw," *IEEE Trans. Geosci. Remote Sens.*, vol. 42, no. 10, pp. 2184–2195, Oct. 2004.

[31] D. Entekhabi, E. G. Njoku, P. E. O'Neill, K. H. Kellogg, W. T. Crow, W. N. Edelstein, J. K. Entin, S. D. Goodman, T. J. Jackson, J. Johnson, J. Kimball, J. R. Piepmeier, R. D. Koster, N. Martin, K. C. McDonald, M. Moghaddam, S. Moran, R. Reichle, J. C. Shi, M. W. Spencer, S. W. Thurman, L. Tsang, and J. Van Zyl, "The soil moisture active passive (SMAP) mission," *Proc. IEEE*, vol. 98, no. 5, pp. 704–716, May 2010.

[32] Y. H. Kerr, P. Waldteufel, J. P. Wigneron, S. Delwart, F. Cabot, J. Boutin, M. J. Escorihuela, J. Font, N. Reul, C. Gruhier, S. E. Juglea, M. R. Drinkwater, A. Hahne, M. Martin-Neira, and S. Mecklenburg, "The SMOS mission: New tool for monitoring key elements of the global water cycle," *Proc. IEEE*, vol. 98, no. 5, pp. 666–687, May 2010.

[33] Y. H. Kerr, P. Waldteufel, J. P. Wigneron, J. M. Martinuzzi, J. Font, and M. Berger, "Soil moisture retrieval from space: The Soil Moisture and Ocean Salinity (SMOS) mission," *IEEE Trans. Geoscience and Remote Sensing*, vol. 39, no. 8, pp. 1729–1735, Aug. 2001.

[34] H. Barre, B. Duesmann, and Y. H. Kerr, "SMOS: The mission and the system," *IEEE Trans. Geosci. Remote Sens.*, vol. 46, no. 3, pp. 587–593, Mar. 2008.

[35] Y. Kerr, J. Font, P. Waldteufel, A. Camps, J. Bara, I. Corbella, F. Torres, N. Duffo, M. Vallilossera, and G. Caudal, "New radiometers: SMOS-a dual pol L-band 2D aperture synthesis radiometer," in *IEEE Aerosp. Conf. Proc.*, 2000, vol. 5, pp. 119–128.

[36] F. Cabot, Y. Kerr, P. Richaume, and P. Waldteufel, "Calibration of localization biases for SMOS," presented at the Proc. IGARSS, Honolulu, HI, 2010.

[37] FAO, UNESCO Soil Map of the World, UNESCO, Rome World Soil Resources Report No. 60, 1988.

[38] V. Masson, J.-L. Champeau, F. Chauvin, C. Meriguet, and R. Lacaze, "A global data base of land surface parameters at 1 km resolution in meteorological and climate models," *J. Climate*, vol. 16, no. 9, pp. 1261–1282, May 2003.

[39] M. C. Dobson, F. T. Ulaby, M. T. Hallikainen, and M. A. Elrayes, "Microwave dielectric behavior of wet soil .2. Dielectric mixing models," *IEEE Trans. Geosci. Remote Sens.*, vol. GRS-23, no. 1, pp. 35–46, Jan. 1985.

[40] M. T. Hallikainen, F. T. Ulaby, M. C. Dobson, M. A. Elrayes, and L. K. Wu, "Microwave dielectric behavior of wet soil .1. Empirical-models and experimental-observations," *IEEE Trans. Geosci. Remote Sens.*, vol. GRS-23, no. 1, pp. 25–34, Jan. 1985.

[41] V. L. Mironov and S. V. Fomin, "Temperature dependable microwave dielectric model for moist soils," in *Proc. PEIRS I, II*, J. A. Kong, Ed., Beijing, China, 2009, pp. 831–835.

[42] V. L. Mironov, L. G. Kosolapova, and S. V. Fomin, "Physically and mineralogically based spectroscopic dielectric model for moist soils," *IEEE Trans. Geosci. Remote Sens.*, vol. 47, no. 7, pp. 2059–2070, Jul. 2009.

[43] V. L. Mironov, L. G. Kosolapova, and S. V. Fomin, "Correction to 'Physically and mineralogically based spectroscopic dielectric model for moist soils' (vol. 47, pg. 2059–2070)," *IEEE Trans. Geosci. Remote Sens.*, vol. 47, no. 7, p. 2085, Jul. 2009.

[44] J. R. Wang and B. J. Choudhury, "Remote-sensing of soil-moisture content over bare field at 1.4 Ghz frequency," *J. Geophys. Res. Oceans Atmos.*, vol. 86, no. C6, pp. 5277–5282, Jun. 1981.

[45] J. R. Wang, E. T. Engman, T. Mo, T. J. Schmugge, and J. C. Shiue, "The effects of soil-moisture, surface-roughness, and vegetation on l-band emission and backscatter," *IEEE Trans. Geosci. Remote Sens.*, vol. GRS-25, no. 6, pp. 825–833, Nov. 1987.

[46] M.-J. Escorihuela, Y. Kerr, J.-P. Wigneron, J.-C. Calvet, and F. Lemaître, "A simple model of the bare soil microwave emission at L-band," *IEEE Geosci. Remote Sens.*, vol. 45, no. 7, pp. 1978–1987, Jul. 2007.

[47] M. J. Escorihuela, A. Chanzy, J. P. Wigneron, and Y. H. Kerr, "Effective soil moisture sampling depth of L-band radiometry: A case study," *Remote Sens. Environ.*, vol. 114, no. 5, pp. 995–1001, May 2010.

[48] R. Panciera, J. P. Walker, and O. Merlin, "Improved understanding of soil surface roughness parameterization for L-band passive microwave soil moisture retrieval," *IEEE Geosci. Remote Sens. Lett.*, vol. 6, no. 4, pp. 625–629, Oct. 2009.

[49] J. P. Wigneron, L. Laguerre, and Y. H. Kerr, "A simple parameterization of the L-band microwave emission from rough agricultural soils," *IEEE Trans. Geosci. Remote Sens.*, vol. 39, no. 8, pp. 1697–1707, Aug. 2001.

[50] B. J. Choudhury, T. J. Schmugge, and T. Mo, "A parameterization of effective soil-temperature for microwave emission," *J. Geophys. Res. Oceans Atmos.*, vol. 87, no. C2, pp. 1301–1304, 1982.

[51] P. de Rosnay and J.-P. Wigneron, "Parameterizations of the effective temperature for L-band radiometry. Inter-comparison and long term validation with SMOSREX field experiment," in *Radiative Transfer Models for Microwave Radiometry*, C. Mätzler, Ed. Stevenage, U.K.: Inst. Elect. Eng., 2005.

[52] T. Mo, B. J. Choudhury, T. J. Schmugge, J. R. Wang, and T. J. Jackson, "A model for microwave emission from vegetation-covered fields," *J. Geophys. Res. Oceans Atmos.*, vol. 87, no. C13, pp. 1229–1237, 1982.

[53] J.-P. Wigneron, M. Pardé, P. Waldteufel, A. Chanzy, Y. Kerr, S. Schmidl, and N. Skou, "Characterizing the dependence of vegetation model parameters on crop structure, view angle and polarization at L-band," *IEEE Trans. Geosci. Remote Sens.*, vol. 42, no. 2, pp. 416–425, Feb. 2004.

[54] J.-P. Wigneron, A. Chanzy, J.-C. Calvet, A. Olioso, and Y. Kerr, "Modeling approaches to assimilating L-band passive microwave observations over land surfaces," *J. Geophys. Res.*, vol. 107, no. D14, p. 4219, Jul. 2002, doi: 10.1029/2001JD000958.

[55] K. Saleh, J.-P. Wigneron, P. de Rosnay, J.-C. Calvet, M. J. Escorihuela, Y. Kerr, and P. Waldteufel, "Impact of rain interception by vegetation and mulch on the L-band emission of natural grass," *Remote Sens. Environ.*, vol. 101, no. 1, pp. 127–139, Mar. 15, 2006, 2006.

[56] J.-P. Wigneron, A. Chanzy, J.-C. Calvet, and N. Bruguier, "A simple algorithm to retrieve soil moisture and vegetation biomass using passive microwave measurements over crop fields," *Remote Sens. Environ.*, vol. 51, no. 1, pp. 331–341, Mar. 1995.

[57] J.-P. Wigneron, J.-C. Calvet, and Y. Kerr, "Monitoring water interception by crop fields from passive microwave observations," *Agric. Forest Meteorol.*, vol. 80, no. 2, pp. 177–194, Jul. 1996.

[58] D. M. Le Vine and M. A. Karam, "Dependence of attenuation in a vegetation canopy on frequency and plant water content," *IEEE Trans. Antennas Propag.*, vol. 34, no. 5, pp. 1090–1096, Sep. 1996.

[59] J. P. Grant, J.-P. Wigneron, A. A. Van de Griend, A. Kruszewsky, S. S. Søbjærg, and N. Skou, "A field experiment on microwave forest radiometry: L-band signal behavior for varying conditions of surface wetness," *Remote Sens. Environ.*, vol. 109, no. 1, pp. 10–19, Jul. 2007.

[60] M. Guglielmetti, M. Schwank, C. Mätzler, C. Oberdörster, J. Vanderborght, and H. Flühler, "FOSMEX: Forest soil moisture experiments with microwave radiometry," *IEEE Trans. Geosci. Remote Sens.*, vol. 46, no. 3, pp. 727–735, Mar. 2008.

[61] P. O'Neill, R. Lang, M. Kurum, A. Joseph, M. Cosh, and T. Jackson, "Microwave soil moisture retrieval under trees using a modified tau-omega model," in *Proc. IGARSS*, Cape Town South, Africa, 2009, pp. III-290–III-293.

[62] R. Rahmoune, P. Ferrazzoli, J. P. Walker, and J. P. Grant, "L-band emission from a Eucalyptus forest in various soil conditions during the NAFE campaign," in *Proc. Micro Rad*, Washington, DC, 2010, pp. 81–85.

[63] E. Santi, S. Paloscia, P. Pampaloni, and S. Pettinato, "Ground-based microwave investigations of forest plots in Italy," *IEEE Trans. Geosci. Remote Sens.*, vol. 47, no. 9, pp. 3016–3025, Sep. 2009.

[64] A. Della Vecchia and P. Ferrazzoli, A Large Scale Approach to Estimate L Band Emission From Forest Covered Surfaces, Tor Vergata Univ., Technical note SO-TN-TV-GS-0001-01.a, 21/02/2006, 2006.

[65] A. Della Vecchia, P. Ferrazzoli, L. Guerriero, R. Rahmoune, S. Paloscia, S. Pettinato, and E. Santi, "Modeling the multi-frequency emission of

broadleaf forests and their components," *IEEE Geosci. Remote Sens.*, vol. 48, no. 1, pp. 260–272, Jan. 2010.
[66] R. Rahmoune and P. Ferrazzoli, Reprocessed Forward Model of L-Band Emission From Broadleaf Forests, 2010, Tor Vergata.
[67] R. Rahmoune and P. Ferrazzoli, Suggested Actions for the Forward Model of Broadleaf Forests, University, Tor Vergata, ESA Technical note 04/06/201, 2010.
[68] A. Della Vecchia and P. Ferrazzoli, A Large Scale Approach to Estimate L Band Emission From Forest Covered Surfaces, Tor Vergata Univ., Rome, DISP Report SMPDD Study, June 2006.
[69] P. Ferrazzoli, L. Guerriero, and J. P. Wigneron, "Simulating L-band emission of forests in view of future satellite applications," *IEEE Trans. Geosci. Remote Sens.*, vol. 40, no. 12, pp. 2700–2708, Dec. 2002.
[70] A. Della Vecchia, P. Ferrazzoli, J.-P. Wigneron, and J. P. Grant, "Modeling forest emissivity at L band and a comparison with multitemporal measurements," *IEEE Geosci. Remote Sens. Lett.*, vol. 4, no. 4, pp. 508–512, Oct. 2007.
[71] C. Mätzler, "Microwave permittivity of dry sand," *IEEE Trans. Antennas Propag.*, vol. 36, no. 1, pp. 317–319, Jan. 1998.
[72] N. R. Peplinski, F. T. Ulaby, and M. C. Dobson, "Dielectric properties of soils in the 0.3-1.3-GHz range," *IEEE Trans. Geosci. Remote Sens.*, vol. 33, no. 3, pp. 803–807, May 1995.
[73] N. R. Peplinski, F. T. Ulaby, and M. C. Dobson, "Corrections to "Dielectric Properties of Soils in the 0.3-1.3-GHz Range"," *IEEE Trans. Geosci. Remote Sens.*, vol. 33, no. 6, p. 1340, Nov. 1995.
[74] F. T. Ulaby, R. K. Moore, and A. K. Fung, *Microwave Remote Sensing—Active and Passive*, vol. 3. Norwood, MA: Artech House, 1986.
[75] L. A. Klein and C. T. Swift, "An improved model for the dielectric constant of sea water at microwave frequencies," *IEEE Trans. Antennas Propag.*, vol. AP-25, no. 1, pp. 104–111, Jan. 1977.
[76] A. Stogryn, "The brightness temperature of a vertically structured medium," *Radio Sci.*, vol. 5, no. 12, pp. 1397–1406, Dec. 1970.
[77] F. Lemaître, J.-C. Poussière, Y. H. Kerr, M. Dejus, R. Durbe, P. de Rosnay, and J.-C. Calvet, "Design and test of the ground based L band radiometer for estimating water in soils (LEWIS)," *IEEE Geosci. Remote Sens.*, vol. 42, no. 8, pp. 1666–1676, Aug. 2004.
[78] Y. H. Kerr, F. Sécherre, J. Lastenet, and J.-P. Wigneron, "Influence of topography on SMOS measurements," in *Proc. Microrad Spec. Meeting*, Rome, Italy, 2004.
[79] ESRI, 2004, World Wivers. [Online]. Available: http://www.lib.unc.edu/reference/gis/datafinder/index.html?individual_datalayer_details=1&data_layer_id=2175
[80] M. Schwank, M. Stähli, H. Wydler, J. Leuenberger, C. Mätzler, and H. Flühler, "Microwave L-band emission of freezing soil," *IEEE Trans. Geosci. Remote Sens.*, vol. 42, no. 6, pp. 1252–1261, Jun. 2004.
[81] [Online]. Available: http://www.natice.noaa.gov/ims/.
[82] P. Waldteufel, J.-L. Vergely, and C. Cot, "A cardioid model for multi-angular radiometric observations," *IEEE Trans. Geosci. Remote Sens.*, vol. 42, no. 5, pp. 1059–1063, May 2004.
[83] T. Pellarin, J. P. Wigneron, J. C. Calvet, M. Berger, H. Douville, P. Ferrazzoli, Y. H. Kerr, E. Lopez-Baeza, J. Pulliainen, L. P. Simmonds, and P. Waldteufel, "Two-year global simulation of L-band brightness temperatures over land," *IEEE Trans. Geosci. Remote Sens.*, vol. 41, no. 9, pp. 2135–2139, Sep. 2003.
[84] R. Oliva, E. Daganzo, Y. Kerr, S. Mecklenburg, S. Nieto, P. Richaume, and C. Gruhier, "SMOS radio frequency interference scenario: Status and actions taken to improve the RFI environment in the 1400–1427-MHz passive band," *IEEE Geosci. Remote Sens.*, vol. 50, no. 5, pp. 1427–1439, May 2012.
[85] R. Rahmoune, P. Ferrazzoli, Y. H. Kerr, and P. Richaume, "Analysis of SMOS signatures over forests and application of L2 algorithm," *Geophys. Res. Abstracts*, vol. 13, p. EGU2011-11692, 2011.
[86] S. Peischl, J. P. Walker, M. Allahmoradi, D. Barrett, R. Gurney, Y. Kerr, E. Kim, J. LeMarshall, C. Rüdiger, D. Ryu, and N. Ye, "Towards validation of SMOS using airborne and ground data over the murrumbidgee catchment," presented at the 18th World IMACS Congr. MODSIM International Congr. Modelling and Simulation, Melbourne, Australia, 2009.
[87] S. Peischl, J. P. Walker, C. Rüdiger, N. Ye, Y. H. Kerr, and E. Kim, "The AACES field experiments: SMOS calibration and validation across the murrumbidgee river catchment," *IEEE Geosci. Remote Sens.*, to be published.
[88] T. J. Jackson, M. H. Cosh, R. Bindlish, P. J. Starks, D. D. Bosch, M. Seyfried, D. C. Goodrich, M. S. Moran, and J. Y. Du, "Validation of advanced microwave scanning radiometer soil moisture products," *IEEE Trans. Geosci. Remote Sens.*, vol. 48, no. 12, pp. 4256–4272, Dec. 2010.
[89] A. Al Bitar, D. Leroux, Y. H. Kerr, O. Merlin, P. Richaume, A. Sahoo, and E. Wood, "Evaluation of SMOS Soil Moisture products over continental U.S. using the SCAN/SNOTEL network," *IEEE Geosci. Remote Sens.*, vol. 50, no. 5, pp. 1572–1586, May 2012.
[90] E. Daganzo, J. Pla, Y. Kerr, M. Martin-Neira, R. Oliva, E. Marelli, S. Mecklenburg, B. Rommen, M. Brown, P. Richaume, and C. Gruhier, "Characterisation of SMOS RF Interferences in the 1400–1427 MHz band as detected during the commissioning phase," *Revue de l'éléctricité et de l'électronique*, vol. 4, pp. 18–29, 2011.

Yann H. Kerr (M'88–SM'01) received the engineering degree from Ecole Nationale Supérieure de l'Aéronautique et de l'Espace, Toulouse, France, the M.Sc. degree in E&EE from Glasgow University, Glasgow, U.K., and Ph.D. degree from Université Paul Sabatier, Toulouse, France.

From 1980 to 1985, he was employed by the Centre National d'Etudes Spatiales, Toulouse, France. In 1985, he joined Laboratoire d'Etudes et de Recherches en Télédétection Spatiale (LERTS) for which he was Director in 1993–1994. He spent 19 months at the Jet Propulsion Laboratory, Pasadena, CA, in 1987–88. He has been working at the Centre d'Etudes Spatiales de la BIOsphère since 1995 (Deputy Director and Director since 2007). His fields of interest are in the theory and techniques for microwave and thermal infrared remote sensing of the Earth, with emphasis on hydrology, water resources management, and vegetation monitoring. He has been involved with many space missions. He was an Earth Observing System (EOS) Principal Investigator (interdisciplinary investigations) and Principal Investigator and precursor of the use of the Scatterometer (SCAT) over land. In 1990, he started work on the interferometric concept applied to passive microwave Earth observation and was subsequently the Science Lead on the Microwave Imaging Radiometer using Image Synthesis (MIRAS) project for European Space Agency (ESA) with Matra Marconi Space and Observatoire Midi Pyrénées. He was also a Co-Investigator on IRIS, OSIRIS, and HYDROS for NASA. He was Science Advisor for Microwave Imaging Multispectral Radiometer (MIMR) and Co-Investigator on Advanced Microwave Scanning Radiometer (AMSR). In 1997, he first proposed the natural outcome of the previous MIRAS work with what was to become the Soil Moisture and Ocean Salinity (SMOS) mission which was eventually selected by ESA in 1999 with him as the SMOS mission Lead-Investigator and Chair of the Science Advisory Group. He is also in charge of the SMOS science activities coordination in France. He has organized all the SMOS Science workshops.

Philippe Waldteufel received the degree from the École Polytechnique, Palaiseau, France, in 1962, and a Doctorat d'État from the Université de Paris, Paris, France, in 1970.

He is a Senior Scientist Emeritus at the Centre National de la Recherche Scientifique. His main scientific interests have been ionospheric and thermospheric physics, radar meteorology, radiowave propagation, macroeconomics, and finally microwave radiometry. He has also served as Director of the Institut de Physique du Globe de Clermont-Ferrand, Deputy Director in the French Weather Service Research Department, and Director for Science in the French Research Ministry. He cosigned to the original Soil Moisture and Ocean Salinity proposal in 1997.

Philippe Richaume received the engineer degree in computer, electronic, and automatic from the Ecole Supérieure d'Informatique, Electronique et Automatique, Paris, France, in 1990, the M.Sc. degree in computer sciences and artificial intelligence from University Paul Sabatier, Toulouse, France, in 1991, and the Ph.D. degree in computer sciences and applied mathematics from Centre Nationale des Arts et Métiers (CNAM), Paris, in 1996.

For the last 20 years, he liked to work in various geophysical labs putting to the test advanced computer science and applied mathematics paradigms against real problems, particularly in the remote sensing context. His domains of interest are nonlinear modeling and inverse problems, particularly using artificial neural networks such as for a radio receiver real-time controller dedicated to solar wind plasma line tracking on-board the WIND/WAVES spacecraft, or for direct-inverse modeling of ocean surface winds from the ERS 1/2 scatterometer or biophysical parameters, Leaf Area Index (LAI), chlorophyl, from POLarization and Directionality of the Earth's Reflectances (POLDER) optical directional reflectance, or using more traditional approaches like for soil moisture retrieval from Soil Moisture and Ocean Salinity brightness temperatures which has been involved with since 2005.

Jean-Pierre Wigneron (SM'03) received the M.Sc./engineering degree from SupAéro, Ecole Nationale Supérieure de l'Aéronautique et de l'Espace, Toulouse, France, in 1987 and the Ph.D. degree from University of Toulouse, Toulouse, France, in 1993.

He is currently a Senior Research Scientist at the Institut National de Recherche Agronomiques (INRA), Bordeaux, France, Co-Coordinator of Remote Sensing activities at INRA and within the Aquitaine Observatoire Aquitain des Sciences de l'Univers (OASU) network, Deputy Director of Ephyse and Head of the remote sensing team. He coordinated the development of the L-band microwave emission of the biosphere model for soil and vegetation in the Level-2 inversion algorithm of the European Space Agency-Soil Moisture and Ocean Salinity mission. His research interests are in microwave remote sensing of soil and vegetation, radiative transfer, and data assimilation. He has more than 100 papers in international peer-reviewed journals, and he has been a member of the Editorial Board of the *International Journal of Microwave Science and Technology* since 2010 and of *Remote Sensing of Environment* since 2005.

Paolo Ferrazzoli (M'94–SM'06) graduated from the University "La Sapienza" of Rome, Rome, Italy, in 1972.

In 1974, he joined Telespazio s.p.a., where he was mainly active in the fields of antennas, slant-path propagation, and advanced satellite telecommunication systems. In 1984, he joined Tor Vergata University of Rome, where he is presently working, teaching microwaves and propagation. His research, here, is focused on microwave remote sensing of vegetated terrains, with particular emphasis on electromagnetic modeling. He has been involved in international experimental remote sensing campaigns such as Agriculture and SAR (AGRISAR), Agriculture and Scatterometer (AGRISCATT), MAESTRO-1, Mutisensor Airborne Campaign (MAC)-Europe, and Shuttle Imaging Radar (SIR)-C/X-Synthertic Aperture Radar (SAR). He has participated to the coordinating team of the European RAdar-Optical Research Assemblage (ERA-ORA) Project, funded by European Economic Community, establishing an assemblage among several European researchers working in radar applications.

Mr. Ferrazzoli has been a member of the Science Advisory Group of the European Space Agency-Soil Moisture and Ocean Salinity Project.

Ali Mahmoodi received the B.Sc., M.Sc., and Ph.D. degrees in computer science from the University of Toronto, Toronto, ON, Canada, in 1989, 1989, and 1996, respectively.

Since 1996, he has worked at Array Systems Computing Inc., Toronto, Canada, as a Software Engineer, Project Scientist, and Project Manager. He taught computer science courses at York University, Toronto, Canada, between 2001 and 2005. His teaching portfolio includes introductory courses in programming languages as well as more advanced courses in software design. He has lead the development and evolution of the Soil Moisture and Ocean Salinity Level 2 Soil Moisture processor for the European Space Agency since 2004. He has managed other remote sensing projects at array including the initial design study for the HYDROS Synthetic Aperture Radar (SAR) processor and the design and the development of an archive system for the Canadian earth observation data, both for the Canadian Space Agency.

Ahmad Al Bitar received the M.E. degree in civil engineering from the Institut National des Sciences Appliquées (INSA), NSA-Lyon, France, in 2003 and the Ph.D. degree in hydrogeology from Institut National Polythechnique de Toulouse, France, in 2006. His thesis work focuses on numerical modeling in stochastic porous media.

In 2006, he joined the Centre d'Etudes Spatiales de la BIOsphère, France. His main research interest is integrated hydrological modeling and assimilation of remote sensing data.

François Cabot received the Ph.D. degree in optical sciences from the University of Paris-Sud, Orsay, France, in 1995.

Between 1995 and 2004, he was with the Centre National d'Etudes Spatiales (CNES) wide-field-of-view instruments quality assessment department, working on absolute and relative calibration of CNES-operated optical sensors over natural terrestrial targets, etc. Since 2004, he joined Centre d'Etudes Spatiales de la BIOsphère as Soil Moisture and Ocean Salinity System Performance Engineer. His research interests are in radiative transfer both optical and microwave and remote sensing of terrestrial surfaces. He has been a Principal and Co-Investigator for various calibration studies for Meteosat Second Generation (MSG), Terra, ENVISAT, and Environment Satellite Advanced Earth Observing Satellite (ADEOS)-II.

Claire Gruhier received the M.S. degree in remote sensing and geographic information system (GIS) applied to environnemental sciences from the Denis Diderot University, Paris, France, in 2006. She is currently working toward the Ph.D. degree at the Centre d'Etudes Spatiales de la BIOsphère, Toulouse, France, and the Pierre et Marie Curie University of Paris IV.

Her research interests focus on validation and intercomparison of soil moisture products based on microwaves measurements over Sahelian area (AMMA sites) in the context of the Soil Moisture and Ocean Salinity mission.

Silvia Enache Juglea received the M.S. degree in microwave, electromagnetism, and optoelectronics from Paul Sabatier University Toulouse, Toulouse, France, in 2007 and the Ph.D. degree in remote sensing from Toulouse University, Toulouse, in 2010.

For 2007 to 2010, she was with the Centre d'Etudes Spatiales de la Biosphère, Toulouse, France, where she was working on the modeling of the surface emission at L-band in the framework of the Soil Moisture and Ocean Salinity (SMOS) mission. Currently, she is working toward the preservation and valorization of remote sensing data at the Centre National d'Etudes Spatiales, Toulouse, France. Her scientific fields of interest include soil moisture and passive microwave modeling in the framework of SMOS mission.

Delphine Leroux received the engineering degree in applied mathematics from the Institut National des Sciences Appliquées, Toulouse, France, in 2009. Since 2009, she has been working toward the Ph.D. degree at the Centre d'Etudes Spatiales de la BIOsphère, Toulouse.

She is currently working on the validation of Soil Moisture and Ocean Salinity data and on statistical methods to construct long and homogeneous time series of soil moisture.

Arnaud Mialon received the M.S. degree in climate and physics-chemistry of the atmosphere from Université Joseph Fourier, Grenoble, France, in 2002, and a Ph.D. degree in ocean-atmosphere-hydrology from Université Joseph Fourier de Grenoble, France and in remote sensing from the Université de Sherbrooke, Sherbrooke, QC, Canada, in 2005.

He joined the Centre d'Etudes Spatiales de la Biosphère, Toulouse, France, in 2006. His fields of interest are focused on passive microwave remote sensing of continental surfaces. He is involved in the Soil Moisture and Ocean Salinity (SMOS) mission as well as the surface Monitoring Of Soil Reservoir EXperiment (SMOSREX) field experiment, where he studies surface soil moisture.

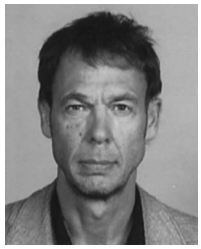

Steven Delwart was born in the U.S., in 1957. He received the B.Sc. honors degree in physics and the M.Sc. degree in optics from the Imperial College, University of London, London, U.K., in 1982.

In 1993, he started his career at Lockheed Missiles and Space Research Laboratories in Palo Alto, CA, in the Advanced Surveillance Department, where he was involved in the development and later made responsible for the calibration of an airborne Infra-Red imaging spectrometer. In 1988, he joined Orlikon-Bhurle Laser division in Switzerland, to develop low-power CO2 laser applications, derived from the Air Defense Anti Tank missile System laser head. In 1993, he joined the European Space Agency as a Performance Engineer for the Medium Resolution Imaging Spectrometer on board ENVISAT, where he was responsible for the development of both the engineering and scientific algorithms, including calibration. His involvement in Soil Moisture and Ocean Salinity (SMOS) started in 2004, with the development of the scientific algorithms, and the coordination of the validation team. He will be managing the algorithm evolution and data product validation activities for SMOS, during the exploitation phase.